The Thesis Committee for Suraj Rajendra Pawar
Certifies that this is the approved version of the following thesis:

Recursive Estimation of Systemic Vascular Resistance Using Measurements From a Left Ventricular Assist Device

APPROVED BY

SUPERVISING COMMITTEE:

Raul G. Longoria, Supervisor

Joseph J. Beaman

Recursive Estimation of Systemic Vascular Resistance Using Measurements From a Left Ventricular Assist Device

by

Suraj Rajendra Pawar

THESIS

Presented to the Faculty of the Graduate School of

The University of Texas at Austin

in Partial Fulfillment

of the Requirements

for the Degree of

Master of Science in Engineering

THE UNIVERSITY OF TEXAS AT AUSTIN

May 2019

Acknowledgments

I would first like to thank my advisor, Prof Raul Longoria, for his guidance, and for letting me be a part of his research group. His class on System Modeling helped me learn Bond Graphs, that were used to develop dynamic equations used in this Thesis. His class on System Identification and estimation helped me develop a deeper understanding of concepts in bayesian estimation. I would also like to thank Prof Joseph Beaman, whose lectures on Stochastic Estimation and Control helped me strengthen foundational concepts in stochastic system modeling and Kalman filtering. I would like to thank the technical director of Windmill Cardiovascular Systems, Jeff Gohean, for providing very useful technical insights related to the cardiovascular system model, estimation theory and for providing experimental data that was used to test the algorithm developed in this Thesis.

No major accomplishment in my life has been possible without the support of friends and family. I would like to thank my wife, Arushi, for ensuring that I do not neglect my health and providing moral support throughout my graduate studies. I want to thank my parents for always encouraging and inspiring me. Finally, I would like to thank my research colleague, Ethan Rapp, who helped this research gain momentum, and offered his time to engage in highly technical discussions.

Recursive Estimation of Systemic Vascular Resistance Using Measurements From a Left Ventricular Assist Device

Suraj Rajendra Pawar, M.S.E
The University of Texas at Austin, 2019

Supervisor: Raul G. Longoria

Cardiovascular disease is the leading cause of deaths worldwide, and one of the ways to treat patients with congestive heart failure is to perform a heart transplant. As the demand for this procedure rises, the disproportionate availability of suitable donors needs to be countered with ways to care and sustain patients who are waiting for a transplant. In this regard, the use of left ventricular assist devices (LVAD) has increased. The research conducted in this Thesis is primarily concerned with the TORVAD ^{TM} (Windmill Cardiovascular Systems In., Austin , TX), a rotary blood pump type LVAD. The load faced by the left ventricle during ejection of blood is termed as Systemic Vascular Resistance (SVR), and is an important parameter that can indicate cardiovascular health. Abnormalities in SVR have been found to be a good indicator of hypertension, heart failure, shock and sepsis. A consistently low SVR can even be a predictor of mortality.

The goal of this Thesis is to investigate ways of recursively estimating SVR in a patient, by using measurements that the TORVAD ™ provides. The Extended Kalman Filter is used to develop an estimation algorithm based on a reduced order model of the cardiovascular system. The estimation accuracy of the algorithm is tested by generating data through simulations of a computational model of the cardiovascular system, and by collecting measurements from the TORVAD ™ while it operates in a mock circulation loop. The algorithm is found to estimate SVR satisfactorily using the available measurements, and is robust to different initial conditions.

Table of Contents

List of Tables

List of Figures

Chapter 1

Introduction

Cardiovascular diseases are the leading cause of deaths globally, and accounted for 31% of the global mortality in the year 2016 [29]. Often a patient with congestive heart failure needs to undergo a heart transplantation. As the demand for heart transplants is increasing, there is a shortage of donors [20]. As a result, there is a wait time during which the heart patient must receive mechanical circulatory support. Technological advancements have made it possible to move away from bulky equipment to implantable devices. Of these, the category of devices that assist the left ventricle by borrowing some blood and pumping it into the Aorta appear to be the most promising [12]. With improvements in the technology of these left ventricular assist devices (LVAD), there is a rise in their use as bridge to transplant (BTT), destination therapy (DT) and bridge to recovery (BTR).

The Toroidal Ventricular Assist device (TORVAD ™; Windmill Cardiovascular Systems In., Austin, TX) is a valveless positive displacement LVAD that can delivery synchronous pulsatile flow to the Aorta. As opposed to continuous flow devices, it offers low shear, preserves the native aortic valve flow, and improves ventricular unloading.[10, 15].

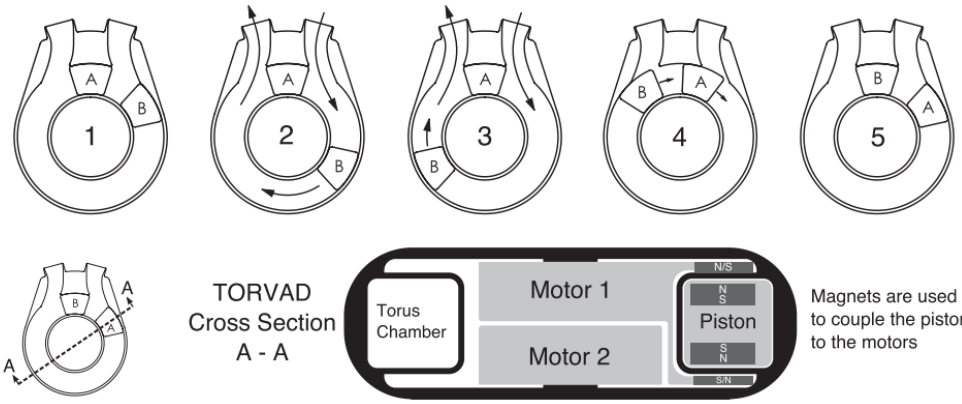

Figure 1.1: Schematic of the TORVAD, showing different modes of operations.

Figure 1.1 shows a schematic of the TORVAD. In the figure, a cross section of the device shows two independently controlled pistons within a torus chamber. The figure also shows the stages involved in one cycle of pumping for the TORVAD. During stages 2 and 3, one piston is stationary while the other moves at a controlled angular velocity to pump blood. The pistons move together during stage 4, and reverse roles by stage 5. The pistons are at rest in Stage 1, which marks the beginning of the next cycle. When a patient is on LVAD support, it is important to monitor his cardiac function and hemodynamic parameters. One such parameter is the Systemic Vascular Resistance (SVR).

SVR is the quantitative value of the left ventricular afterload. It is the aggregate resistance to blood flow posed by the systemic circulation. SVR can be defined by the following equation.

$$SVR = \frac{MAP - CVP}{CO} \tag{1.1}$$

In this expression, MAP is the Mean Arterial Pressure (mmHg), CVP is the Central Venous Pressure (mmHg) and CO is the cardiac output (mL/s). It is common to report SVR in units of mmHg-s/mL. Abnormalities in the value of SVR are commonly associated with diseases such as hypertension, congestive heart failure, shock and sepsis. A consistently low SVR over a 24 hour period can even be a strong predictor of mortality [23, 17, 19, 25].

Traditionally, SVR measurement requires arterial and venous cannulation to measure pressure and cardiac output. There have been some advances made in the non invasive measurement of SVR [1, 25], however they require the patient to be in the clinic, and rely on Doppler or ultrasound based sensors. Considerable research has been done to develop electric analog models of the cardiovascular system and to estimate their parameters, which in turn can help estimate hemodynamic parameters, such as SVR [22, 26, 28, 18, 31]. The research done by *Yu et al.* [31] and *Ruchti et al.* [22] is especially of interest, since they use measurements from the LVAD, along with aortic pressure or flow measurements to estimate systemic circulation parameters.

Besides monitoring the patients health, estimating SVR could also be useful in designing feedback controllers for LVADs. Most continuous flow LVADs are tuned for a certain flow rate by physicians in the clinic. In the case of the TORVAD $^{\text{TM}}$, the controller tracks predefined trajectories for each piston. In the future, if these devices are to be used for permanent implantation, it is necessary to design a feedback controller that can sense hemodynamic variables, such as SVR, and adjust the pump's operation to mimick the

physiological response of a natural heart. For instance, in the natural heart, a consequence of increased ventricular afterload (indicated by increased SVR) is an increase in the cardiac output due to the Frank Starling mechanism [14]. There is ongoing research in designing closed loop control systems for LVADs, some of which rely on estimates of SVR [24, 30, 5, 2].

The goal of this Thesis is to investigate recursive estimation of SVR using only the measurements provided by the TORVAD ™. The estimation algorithm follows methodology developed by *Yu et al.* [31], and uses an Extended Kalman Filter (EKF) based on a reduced order model of the cardiovascular system. The EKF is chosen for its ability to estimate states and parameters of a system, and also quantify the error in these estimates, thereby giving us a measure of the confidence in estimates. Chapter 2 introduces a reduced order model that is used to design the EKF algorithm. It also discusses a higher order model that will be used to generate simulated measurements for testing the EKF algorithm. Chapter 3 develops the equations of the EKF algorithm when it is applied to the reduced order model derived in Chapter 2. For deterministic systems, the ability to reconstruct states from output measurements is analyzed using principles of observability. However, for systems riddled with process and measurement noise, these concepts must be replaced with ones of stochastic observability [8]. Chapter 4 uses concepts of Identifiability [13] to determine the ability to estimate SVR by using measurements provided by the TORVAD ™. The use of stochastic observability concepts to study the Estimability [3] of the EKF algorithm is also discussed in this

Chapter, thereby gauging its ability to estimate system states and parameters. Chapter 5 and 6 show results from simulation studies, and experiments conducted using a mock circulation loop that runs a 12-state computational model [11] of the cardiovascular system. Chapter 7 is the final chapter and summarizes the performance of the EKF algorithm while estimating SVR, and presents possible extensions of the work in future.

Chapter 2

Electric Analog of the Cardiovascular System

It is very common to represent the cardiovascular system (CVS) using electrical elements. Table 2.1 summarizes the analogy between these elements and physiology of the CVS [30].

Electric Element	**CVS analogy**
Resistors (R)	Viscous dissipation in blood flow
Capacitors (C)	Elastic properties of vessel walls
Inductors (L)	Inertial properties of blood flow
Diodes (D)	Unidirectional heart valves

Table 2.1: Analogy between electric elements and physiology of CVS

Two models with varying levels of complexity are used in this Thesis. The more complex model comprises of 12 states, and is used to simulate measurements of differential pressure and VAD flow. The EKF algorithm discussed in Chapter 3 however, is designed around a reduced order model comprising of 4 states. Each of these models is discussed in the following sections.

2.1 Computational model

It is becoming increasingly common to simulate the cardiovascular system on a mock circulation loop. Such a setup offers the advantage of con-

necting an LVAD, and performing hardware in the loop tests, thereby accelerating development and testing of algorithms to be deployed on the LVAD. The models that need to run on such a mock circulation loop, are typically of high fidelity so as to replicate most nuances of the actual cardiovascular system. One such model is reported by *Gohean et al.* [11], and has been found to replicate the dynamics of the cardiovascular system satisfactorily. A circuit representation of the model, hereby referred to as the 'computational model' is shown in figure 2.1.

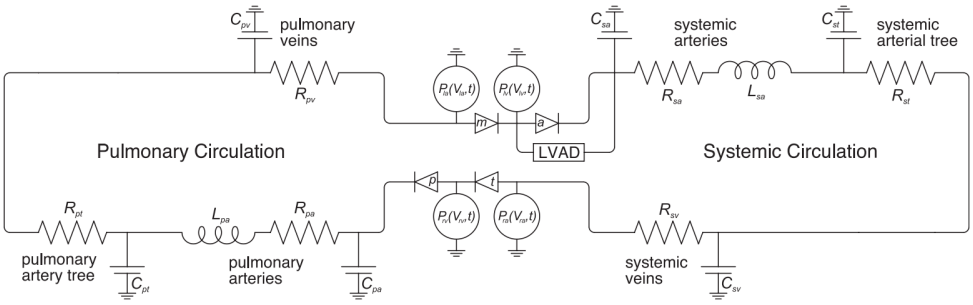

Figure 2.1: Electric circuit representation of the computational model

In the computational model, each heart chamber generates pressure that is made up of an active, and a passive component. The LVAD is treated as a flow source, and both systemic and pulmonary circulation circuits are represented by a network of electrical elements. The value of each element is summarized in Appendix A. For this Thesis, the computational model is simulated in the commercial software MATLAB Release 2018b (The MathWorks, Inc., Natick, Massachusetts, United States). Data collected from this simulation is used to run tests described in Chapter 5. The TORVAD ^{TM} is then

connected to a mock circulation loop which runs the computational model, and data from this experiment is used for tests described in Chapter 6.

2.2 Reduced order model

The EKF algorithm needs a model of the system to propagate states and their error covariances. It then uses measurements to correct these estimates using a 'measurement update' step. The selection of the model is important and requires careful trade off between fidelity and computational ease. The computational model replicates CVS dynamics well, but is not the ideal choice for an algorithm that is intended for deployment on an embedded controller. Since we only have one measurement (differential pressure ΔP), we must seek a model that has minimal number of states, and delivers satisfactory dynamics for the purpose of estimation.

Several reduced order models of the CVS are available in the literature. In most of these models, the systemic circulation is represented by a Windkessel, with 2,3, or 4 elements [28, 6]. The four element Windkessel has been found to satisfactorily replicate necessary dynamics of the Systemic Circulation over a considerable range of frequencies (3 - 12 Hz). In these models, the pulmonary circulation has been modeled either as a pressure source [30], or as a constant capacitor [31]. The electric model used for the EKF algorithm formulation in this Thesis is based on *Yu et al.* [31], with the key difference being the absence of an explicit model of the LVAD. This is possible because of the TORVAD's ™ embedded controller being able to estimate both pump

flow (Q_{vad}) and differential pressure (ΔP) without the use of additional sensors [9]. This model, hereby referred to as the 'reduced order model', is shown in figure 2.2. The specific meaning of each element in the model is summarized in table 2.2.

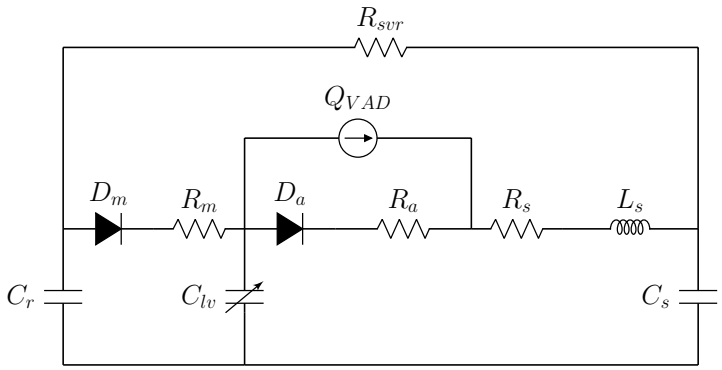

Figure 2.2: Electric circuit representation of the reduced order model

Electric Element	**CVS analogy**
D_a, D_m	Aortic and mitral valves modeled as ideal diodes
R_a, R_m	Aortic and mitral valve resistance
Q_{vad}	Known flow source
R_s	Characteristic resistance of the aorta
L_s	Aortic inductance
R_{svr}	Systemic Vascular Resistance
C_r	Pulmonary circulation compliance
C_s	Systemic circulation compliance
C_{lv}	Left ventricle as time varying capacitor

Table 2.2: Reduced order model elements and their meaning

The presence of ideal diodes in the model necessitates the need to switch between discrete stages of the cardiac cycle. Each stage corresponds to a

specific configuration of the diodes. A diode that is on (D_a or $D_m = 1$), results in flow of blood. A diode that is off (D_a or $D_m = 0$), blocks the flow of blood. The model for each stage has the same state vector, which can be written as follows

$$\boldsymbol{x} = \begin{bmatrix} V_s & V_r & V_{lv} & Q_{ao} \end{bmatrix}^T \tag{2.1}$$

In the above equation, V_s, V_r and V_{lv} represent the volume of blood in the systemic circulation, pulmonary circulation and left ventricle respectively. Q_{ao} represents the aortic blood flow rate. Pressures can be calculated using these states by using equation (2.2).

$$\begin{aligned} P_s &= \frac{V_s}{C_s} \\ P_r &= \frac{V_r}{C_r} \end{aligned} \tag{2.2}$$

Table 2.3 summarizes diode values and switching criteria for each stage.

Stage	**Diodes**	**Switching criteria**
Ejection	$D_a = 1,\ D_m = 0$	$P_{lv} > P_{ao},\ P_{lv} > P_r,\ Q_{ao} > 0$
Filling	$D_a = 0,\ D_m = 1$	$P_{lv} \leq P_{ao},\ P_{lv} \leq P_r,\ Q_{ao} \leq 0$
Isovolumic expansion/contraction	$D_a = 0,\ D_m = 0$	$P_r \leq P_{lv} <= P_{ao}, Q_{ao} \leq 0$

Table 2.3: Switching criteria and stages for reduced order model

2.2.1 Left Ventricle Pressure

Based on the approach taken by *Yu et al.* [31], the left ventricle in the reduced order model is represented by a time varying capacitor. The pressure

is then calculated using equation (2.3).

$$P_{lv} = E(t)(V_{lv} - V_0) \tag{2.3}$$

In the above equation, V_0 represents the volume of blood in the unstressed left ventricle, and is kept at 5 mL [11]. The elastance value at any given time is obtained by scaling a normalized elastance curve (figure 2.3) in time, and amplitude. Given the heart rate (HR), we can scale the current time t to normalized time t_n by using equation 2.4.

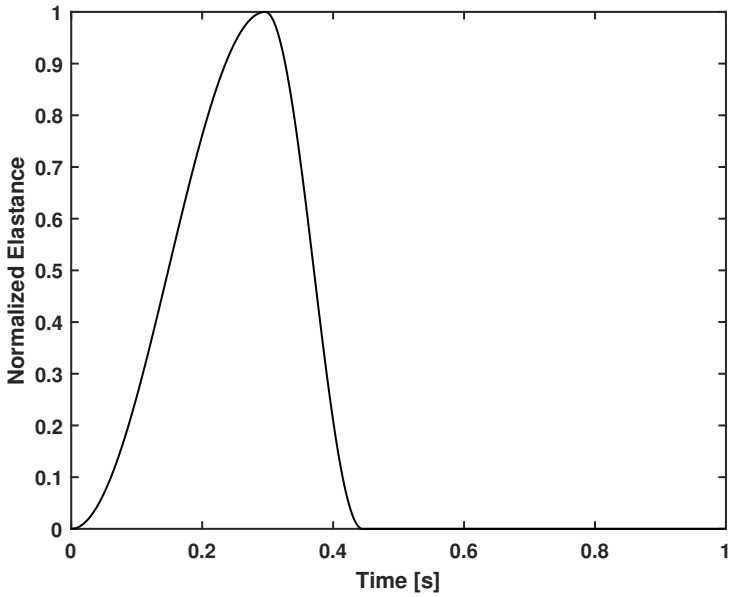

Figure 2.3: Normalized elastance curve

$$t_n = \text{mod}(t, t_c) \tag{2.4}$$

In the above equation, mod represents the modulo function and calculates the remainder when two numbers are divided. t_c represents the time required for one cardiac cycle and is given by equation 2.5.

$$t_c = \frac{60}{\text{HR}} \tag{2.5}$$

Elastance is then calculated using equation 2.6.

$$E(t) = (E_{max} - E_0)\, e(t_n) + E_0 \tag{2.6}$$

In the above equation, E_{max} and E_0 are the maximum and minimum values of the left ventricle elastance and are fixed at 3.25 mL/mmHg and 0.0068 mL/mmHg respectively for a healthy heart. $e(t_n)$ represents the value of the normalized elastance at the normalized time, and is calculated using equation 2.7 [11].

$$e(t_n) = \begin{cases} \frac{1}{2} - \frac{1}{2}\cos\left(\frac{3\pi t_n}{2t_s}\right) & \text{if } 0 \leq t_n < \frac{2}{3}t_s \\ \frac{1}{2} + \frac{1}{2}\cos\left(\frac{3\pi t_n}{t_s} - 2\pi\right) & \text{if } \frac{2t_s}{3} \leq t_n < t_s \\ 0 & \text{if } t_n > t_s \end{cases} \tag{2.7}$$

In the above equation, t_s is ventricular contraction time, and is given by equation (2.8) [11]:

$$t_s = \frac{550 - 1.75\ \text{HR}}{1000} \tag{2.8}$$

Equation (2.3) makes it possible to calculate the normalized elastance in real-time, without the need of interpolating a curve as is the case in *Yu et al* [31].

2.2.2 Ejection

During ejection, the aortic valve is open ($D_a = 1$) and the mitral valve is closed ($D_m = 0$). A bond graph of this stage is shown in figure 2.4.

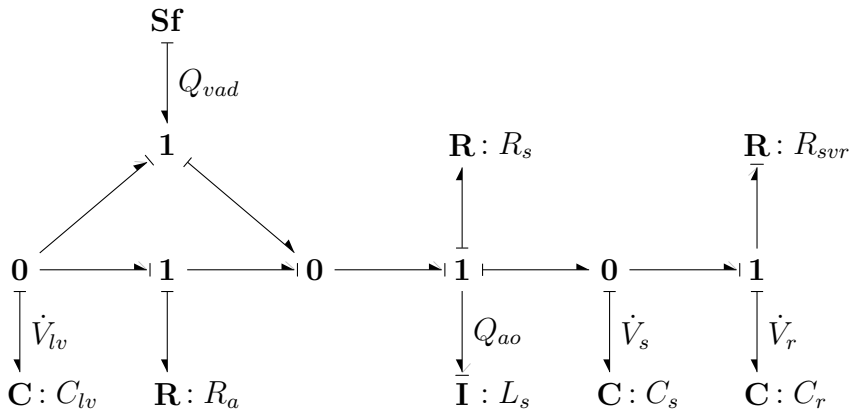

Figure 2.4: Bond graph of the reduced order model during ejection

State equations for this stage can be written as follows.

$$\begin{aligned}
\dot{V}_s &= Q_{ao} - \frac{1}{R_{svr}}\left(\frac{V_s}{C_s} - \frac{V_r}{C_r}\right) \\
\dot{V}_r &= \frac{1}{R_{svr}}\left(\frac{V_s}{C_s} - \frac{V_r}{C_r}\right) \\
\dot{V}_{lv} &= -Q_{ao} \\
\dot{Q}_{ao} &= \frac{1}{L_s}\left(E(t)(V_{lv} - V_0) - R_a(Q_{ao} - Q_{vad}) - R_s Q_{ao} - P_s\right)
\end{aligned} \tag{2.9}$$

Measurement of differential pressure can be represented by the following equa-

tion.

$$\Delta P = R_a(Q_{ao} - Q_{vad}) \tag{2.10}$$

2.2.3 Filling

During the filling stage, the aortic valve is closed ($D_a = 0$), and the mitral valve is open ($D_m = 1$). A bond graph of this stage is shown in figure 2.5.

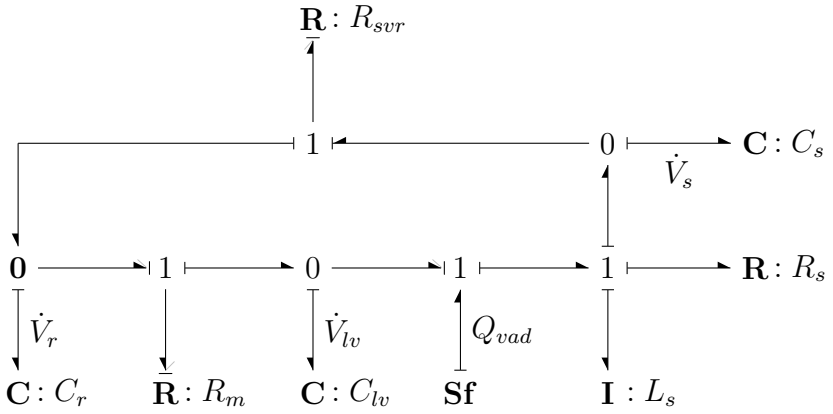

Figure 2.5: Bond graph of reduced order model during filling

The model dynamics are governed by the following state equations during this stage.

$$\begin{aligned}
\dot{V}_s &= Q_{vad} - \frac{1}{R_{svr}}\left(\frac{V_s}{C_s} - \frac{V_r}{C_r}\right) \\
\dot{V}_r &= \frac{1}{R_{svr}}\left(\frac{V_s}{C_s} - \frac{V_r}{C_r}\right) - \frac{1}{R_m}\left(\frac{V_r}{C_r} - E(t)(V_{lv} - V_0)\right) \\
\dot{V}_{lv} &= \frac{1}{R_m}\left(\frac{V_r}{C_r} - E(t)(V_{lv} - V_0)\right) - Q_{vad} \\
\dot{Q}_{ao} &= \dot{Q}_{vad}
\end{aligned} \tag{2.11}$$

Measurement of differential pressure can be written as follows.

$$\Delta P = E(t)(V_{lv} - V_0) - (L_s\dot{Q}_{vad} + R_sQ_{vad} + V_s/C_s) \tag{2.12}$$

2.2.4 Isovolumic Expansion/Contraction

During the isovolumic contraction or expansion stage, both the aortic and mitral valves are closed ($D_a = 0$ and $D_m = 0$). A bond graph of this stage is shown in figure 2.6.

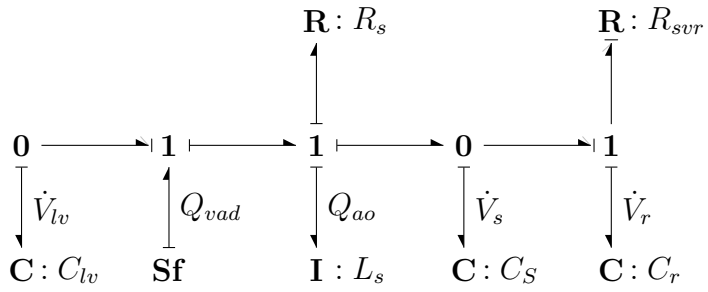

Figure 2.6: Bond graph of the reduced order model during isovolumic phases

Model dynamics during this stage are governed by the following equations.

$$\begin{aligned}
\dot{V}_s &= Q_{vad} - \frac{1}{R_{svr}}\left(\frac{V_s}{C_s} - \frac{V_r}{C_r}\right) \\
\dot{V}_r &= \frac{1}{R_{svr}}\left(\frac{V_s}{C_s} - \frac{V_r}{C_r}\right) \\
\dot{V}_{lv} &= -Q_{vad} \\
\dot{Q}_{ao} &= \dot{Q}_{vad}
\end{aligned} \tag{2.13}$$

Measurement of differential pressure can be written as follows.

$$\Delta P = E(t)(V_{lv} - V_0) - (L_s\dot{Q}_{vad} + R_sQ_{vad} + V_s/C_s) \tag{2.14}$$

2.2.5 Selection of nominal parameter values - Impedance Analysis

Before we simulate the reduced order model and test the accuracy of the estimation algorithm in predicting parameter values, we need to ensure that we have a good sense of the actual nominal values of these parameters. These values must be selected such that the reduced order model generates pressures and volumes as close as possible to the computational model. The level of confidence to placed on the model can be tuned in the EKF algorithm, and deviations from the computational model are expected to be corrected by utilizing information from the measurements to update parameter and state estimates.

The parameter values were tuned by matching the impedance of the systemic circulation circuit of the computational and reduced order model. This process allows for tuning of systemic circulation compliance C_s, characteristic aortic resistance R_s and aortic inductance L_s. The value of SVR was calculated using equation (1.1). The pulmonary circulation compliance C_r and mitral valve resistance R_m were kept same as in *Yu et al* [31]. The aortic valve resistance, R_a, was taken from *Gohean et al* [11].

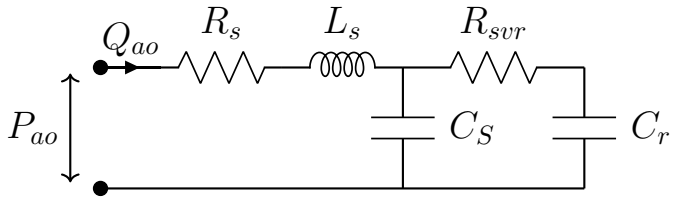

Figure 2.7: Systemic circulation circuit of reduced order model

For the reduced order model, the systemic circulation circuit shown in figure 2.7 can be used to calculate the effective impedance faced by the left ventricle while ejecting blood. The transfer function between the aortic pressure P_{ao} and aortic flow Q_{ao} can be expressed as follows.

$$\frac{P_{ao}(s)}{Q_{ao}(s)} = \frac{a_1 s^3 + a_2 s^2 + a_3 s + 1}{b_1 s^2 + b_2 s} \tag{2.15}$$

Where

$$\begin{aligned} a_1 &= L_s R_{svr} C_s C_r \\ a_2 &= R_{svr} R_s C_s C_r + L_s C_s + L_s C_r \\ a_3 &= R_s C_s + R_s C_r + R_{svr} C_r \\ b_1 &= R_{svr} C_s C_r \\ b_2 &= C_s + C_r \end{aligned} \tag{2.16}$$

The impedance can then be expressed as :

$$Z_{red}(j\omega) = \left| \frac{P_{ao}(j\omega)}{Q_{ao}(j\omega)} \right| \tag{2.17}$$

Figure 2.8 shows the systemic circulation circuit of the computational model. The transfer function between the aortic pressure P_{ao} and aortic flow Q_{ao} can be expressed as follows.

$$\frac{P_{ao}(s)}{Q_{ao}(s)} = \frac{p_1 s^3 + p_2 s^2 + p_3 s + p_4}{q_1 s^4 + q_2 s^3 + q_3 s^2 + q_4 s + 1} \tag{2.18}$$

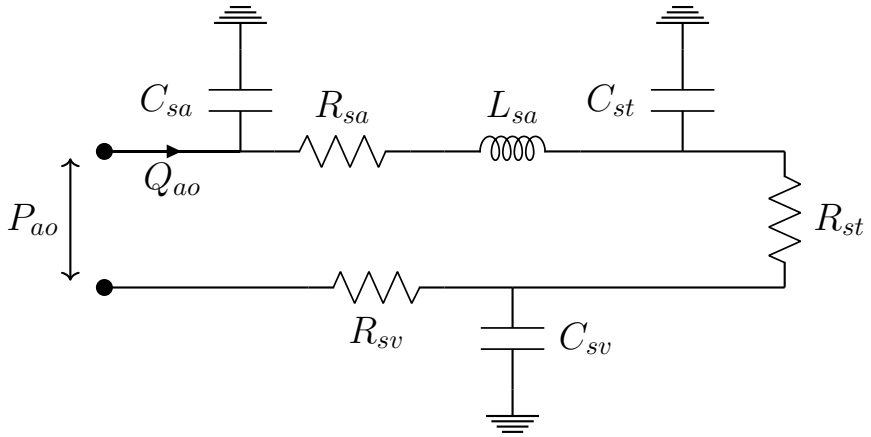

Figure 2.8: Systemic circulation circuit of computational model.

Where

$$
\begin{aligned}
p_1 &= C_{st}C_{sv}L_{sa}R_{st}R_{sv} \\
p_2 &= C_{st}L_{sa}R_{st} + C_{st}L_{sa}R_{sv} + C_{sv}L_{sa}R_{sv} + C_{st}C_{sv}R_{sa}R_{st}R_{sv} \\
p_3 &= L_{sa} + C_{st}R_{sa}R_{st} + C_{st}R_{sa}R_{sv} + C_{sv}R_{sa}R_{sv} + C_{sv}R_{st}R_{sv} \\
p_4 &= R_{sa} + R_{st} + R_{sv} \\
q_1 &= C_{sa}C_{st}C_{sv}L_{sa}R_{st}R_{sv} \\
q_2 &= C_{sa}C_{st}L_{sa}R_{st} + C_{sa}C_{st}L_{sa}R_{sv} + C_{sa}C_{sv}L_{sa}R_{sv} + C_{sa}C_{st}C_{sv}R_{sa}R_{st}R_{sv} \\
q_3 &= C_{sa}L_{sa} + C_{sa}C_{st}R_{sa}R_{st} + C_{sa}C_{st}R_{sa}R_{sv} + C_{sa}C_{sv}R_{sa}R_{sv} \\
&\quad + C_{sa}C_{sv}R_{st}R_{sv} + C_{st}C_{sv}R_{st}R_{sv} \\
q_4 &= C_{sa}R_{sa} + C_{sa}R_{st} + C_{sa}R_{sv} + C_{st}R_{st} + C_{st}R_{sv} + C_{sv}R_{sv}
\end{aligned}
\tag{2.19}
$$

The transfer function is given by a similar expression as equation (2.17). All the values obtained are summarized in table 2.4. Figure 2.9 shows the

impedance curves of the reduced order model and the computational model with these parameters, for a healthy person and one with critical heart failure.

Element	Healthy	Heart Failure	Units
R_s	0.02	0.0398	mmHg-s/mL
R_a	0.0025	0.0025	mmHg-s/mL
R_m	0.005	0.005	mmHg-s/mL
R_{svr}	0.975	1.07	mmHg-s/mL
L_s	0.0002	0.0005	mmHg-s^2/mL
C_r	4.4	4.4	mL/mmHg
C_s	1.5	0.65	mL/mmHg

Table 2.4: Values of the reducced order model parameters used for a healthy person

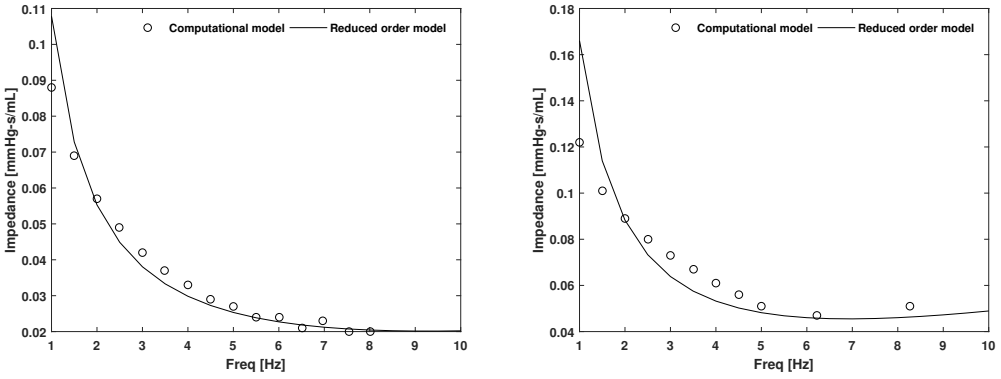

(a) (b)

Figure 2.9: Impedance curves for a (a) healthy person and a person with (b) critical heart failure

2.2.6 Simulation of reduced order model

The state equations for the reduced order model were simulated in MATLAB Release 2018b (The Mathworks, Inc., Natick, Massachusetts, United

States) using Euler integration and a time step of 0.0001 ms. The reduced order model is found to sufficiently replicate all necessary dynamics of the computational model. The left ventricle pressure, aortic pressure, atrial pressure, aortic flow and left ventricle volume are shown in figure 2.10. The initial conditions used for the states of the reduced order model for each simulation run are summarized in Appendix B.

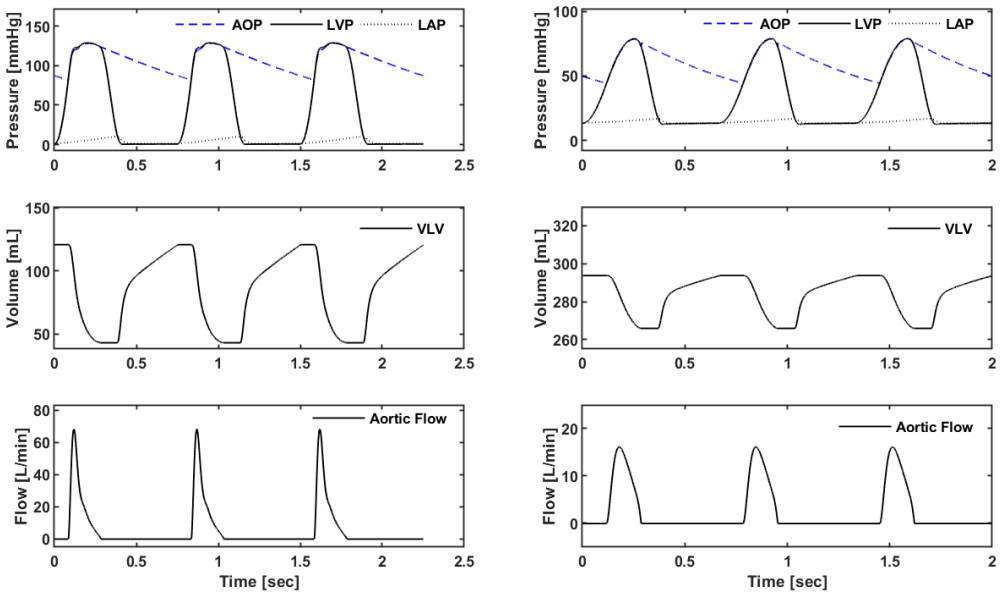

(a) (b)

Figure 2.10: Pressures, Left ventricle volume and aortic flows for a (a) healthy human at 80 bpm, and (b) critical heart failure at 90 bpm simulated without VAD support.

2.3 Summary

This chapter introduced two models of the CVS that will be used throughout the Thesis. The first model, termed the 'Computational Model', comprises of 12 states. This model will be simulated with a continuous VAD flow rate, and the differential pressure generated will be treated as measurement data. These measurements will then be corrupted by additive white Gaussian noise before they are used in the Extended Kalman Filter. Chapter 5 and 6 discuss the tests done on the EKF algorithm using simulated and experimentally collected measurements.

A second model, termed as the 'Reduced order model' was also discussed. This model is used to formulate the EKF equations, as described in Chapter 3. The reduced order model has 4 states and is able to satisfactorily replicate the dynamics of the computational model. This chapter also derived the model equations, which are different for each stage of the cardiac cycle. The state of the heart valves dictates the stage of the cardiac cycle, and for each stage, a bond graph representation of the system was shown. The parameters to be used for the reduced order model were tuned by matching the impedance as seen by the left ventricle, in the computational and reduced order model. This was done for a healthy heart, and one with critical failure, without VAD support. Finally, results from a simulation of the reduced order model were shown.

Chapter 3

Extended Kalman Filter for SVR estimation

The Extended Kalman Filter (EKF) is an extension of the Kalman filter for non linear dynamic systems. It has been used successfully in many applications for both state and parameter estimation [16]. For such problems, EKF is the most optimal linear estimator. It must be noted, however, that there could be nonlinear estimators more optimal than the EKF.

The algorithm uses knowledge of the model dynamics to propagate the mean and covariance of the states, conditioned on past measurements. It can then update these statistics by using the most recent measurement, thereby giving us the most likely value of the states (used as the state estimate) and the level of confidence on these values. It allows us to tune the amount of process uncertainty present in the form of noise and modeling errors, and measurement uncertainties, to produce an overall estimate that is more accurate than just the process or measurements. Being recursive in nature, the algorithm is well suited for implementation in a real time environment, such as a micro-controller. The following sections discuss the equations of the algorithm in further detail.

3.1 EKF equations

The continuous-discrete form of the EKF is used for this Thesis. The continuous dynamics of the model are used to propagate the states and covariance forward in time, and discrete measurements are used to correct them with a 'measurement update' step. The equations for the algorithm are summarized in table 3.1 [8].

System Model Measurement Model	$\dot{\boldsymbol{x}}(t) = \boldsymbol{f}(\boldsymbol{x}(t), t) + \boldsymbol{w}(t); \quad \boldsymbol{w}(t) \sim N(\boldsymbol{0}, Q(t))$ $\boldsymbol{z}_k = \boldsymbol{h}_k(\boldsymbol{x}(t_k)) + \boldsymbol{v}_k;\ k = 1, 2, \ldots; \quad \boldsymbol{v}_k \sim N(\boldsymbol{0}, R_k)$
Initial Conditions Other Assumptions	$\boldsymbol{x}(0) \sim N(\hat{\boldsymbol{x}}_0, P_0)$ $E\left[\boldsymbol{w}(t)\boldsymbol{v}_k^T\right] = 0$ for all k and t
State Estimate Propagation Error Covariance Propagation	$\dot{\hat{\boldsymbol{x}}}(t) = \boldsymbol{f}(\hat{\boldsymbol{x}}(t), t)$ $\dot{P}(t) = F(\hat{\boldsymbol{x}}(t), t)P(t) + P(t)F(\hat{\boldsymbol{x}}(t), t)^T + Q(t)$
State Estimate Update Error Covariance Update Gain Matrix	$\hat{\boldsymbol{x}}_k^+ = \hat{\boldsymbol{x}}_k^- + K_k[\boldsymbol{z}_k - \boldsymbol{h}_k(\hat{\boldsymbol{x}}_k^-)]$ $P_k^+ = [I - K_k H_k(\hat{\boldsymbol{x}}_k^-)]P_k^-$ $K_k = P_k^- H_k^T(\hat{\boldsymbol{x}}_k^-)\left[H_k(\hat{\boldsymbol{x}}_k^-)P_k H_k(\hat{\boldsymbol{x}}_k^-)^T + R_k\right]^{-1}$
Definitions	$F(\hat{\boldsymbol{x}}(t), t) = \left.\dfrac{\partial \boldsymbol{f}(\boldsymbol{x}(t), t)}{\partial \boldsymbol{x}(t)}\right\rvert_{\boldsymbol{x}(t)=\hat{\boldsymbol{x}}(t)}$ $H_k(\hat{\boldsymbol{x}}^-) = \left.\dfrac{\partial \boldsymbol{h}_k(\boldsymbol{x}(t_k))}{\partial \boldsymbol{x}(t_k)}\right\rvert_{\boldsymbol{x}(t_k)=\hat{\boldsymbol{x}}^-}$

Table 3.1: Continuous - Discrete EKF equations.

The reduced order model of the CVS, as introduced in Chapter 2, is linear. In order to estimate unknown parameters of the model, the state vector can be augmented by adding an additional state for the parameter, that has no dynamics [8].

$$\dot{R}_{svr} = 0 \tag{3.1}$$

$$\boldsymbol{x}_{aug} = \begin{bmatrix} V_s & V_r & V_{lv} & Q_{ao} & R_{svr} \end{bmatrix}^T \tag{3.2}$$

The addition of this state, makes the model nonlinear. When the EKF equations shown above are used for the reduced order model, the states vector is $\boldsymbol{x}_{aug}$. The nonlinear system dynamics can then be represented by the following state space representation :

$$\begin{aligned} \dot{\boldsymbol{x}}_{aug}(t) &= \boldsymbol{f}(\boldsymbol{x}_{aug}(t), u(t), t) \\ y(t) &= h(\boldsymbol{x}_{aug}(t), u(t), t) \end{aligned} \tag{3.3}$$

To ensure faster convergence of the filter, the total volume of blood in the model was held constant at a value represented by V_{total} [31]. At each measurement update step, the following equations were used to adjust the volume in the pulmonary circulation represented by the capacitor C_r.

$$\begin{aligned} \hat{V}_r &= \hat{V}_r + (V_{\text{total}} - V_{\text{sum}}) \\ V_{\text{sum}} &= \hat{V}_s + \hat{V}_r + \hat{V}_{lv} \end{aligned} \tag{3.4}$$

The linearized matrices F and H_k govern the dynamics of the linearized system, which can be represented by the standard linear state space form.

$$\begin{aligned} \dot{\boldsymbol{x}}_{aug}(t) &= F\boldsymbol{x}_{aug}(t) + Bu(t) \\ y_k &= H_k\boldsymbol{x}_{aug}(t) + D_k u(t) \end{aligned} \tag{3.5}$$

Note that during each time step, the value of the left ventricle elastance, $E(t_k)$ is held constant. The functions and matrices involved in eqs. (3.3) and (3.5) are summarized below.

3.1.1 Ejection

The nonlinear functions $\boldsymbol{f}$, h, and the linearized matrices F and H_k for this stage are as follows.

$$
\begin{aligned}
\boldsymbol{f} &= \begin{bmatrix} -\dfrac{1}{R_{svr}}\left(\dfrac{V_s}{C_s} - \dfrac{V_r}{C_r}\right) + Q_{ao} \\ \dfrac{1}{R_{svr}}\left(\dfrac{V_s}{C_s} - \dfrac{V_r}{C_r}\right) \\ -Q_{ao} \\ \dfrac{1}{L_s}\left(E(t_k)(V_{lv} - V_0) - R_a(Q_{ao} - Q_{vad}) - R_s Q_{ao} - \dfrac{V_s}{C_s}\right) \\ 0 \end{bmatrix} \\
h &= R_a(Q_{ao} - Q_{vad}) \\
F &= \begin{bmatrix} -\dfrac{1}{C_s R_{svr}} & \dfrac{1}{C_r R_{svr}} & 0 & 1 & -\dfrac{1}{R_{svr}^2}\left(\dfrac{V_r}{C_r} - \dfrac{V_s}{C_s}\right) \\ \dfrac{1}{C_s R_{svr}} & -\dfrac{1}{C_s R_{svr}} & 0 & 0 & \dfrac{1}{R_{svr}^2}\left(\dfrac{V_r}{C_r} - \dfrac{V_s}{C_s}\right) \\ 0 & 0 & 0 & -1 & 0 \\ -\dfrac{1}{C_s L_s} & 0 & \dfrac{E(t_k)}{L_s} & -\dfrac{R_a + R_s}{L_s} & 0 \\ 0 & 0 & 0 & 0 & 0 \end{bmatrix} \\
H_k &= \begin{bmatrix} 0 & 0 & 0 & R_a & 0 \end{bmatrix}
\end{aligned}
\tag{3.6}
$$

3.1.2 Filling

The nonlinear functions $\boldsymbol{f}$, h, and the linearized matrices F and H_k for this stage are as follows.

$$
\begin{aligned}
\boldsymbol{f} &= \begin{bmatrix}
-\dfrac{1}{R_{svr}}\left(\dfrac{V_s}{C_s}-\dfrac{V_r}{C_r}\right)+Q_{vad} \\
\dfrac{1}{R_{svr}}\left(\dfrac{V_s}{C_s}-\dfrac{V_r}{C_r}\right)-\dfrac{1}{R_m}\left(\dfrac{V_r}{C_r}-E(t_k)(V_{lv}-V_0)\right) \\
\dfrac{1}{R_m}\left(\dfrac{V_r}{C_r}-E(t_k)(V_{lv}-V_0)\right)-Q_{vad} \\
\dot{Q}_{vad} \\
0
\end{bmatrix} \\
h &= E(t_k)(V_{lv}-V_0)-(L_s\dot{Q}_{vad}+V_s/C_s) \\
F &= \begin{bmatrix}
-\dfrac{1}{C_sR_{svr}} & \dfrac{1}{C_rR_{svr}} & 0 & 0 & -\dfrac{1}{R_{svr}^2}\left(\dfrac{V_r}{C_r}-\dfrac{V_s}{C_s}\right) \\
\dfrac{1}{C_sR_{svr}} & -\dfrac{1}{C_rR_m}-\dfrac{1}{C_rR_{svr}} & \dfrac{E(t_k)}{R_m} & 0 & \dfrac{1}{R_{svr}^2}\left(\dfrac{V_r}{C_r}-\dfrac{V_s}{C_s}\right) \\
0 & \dfrac{1}{C_rR_m} & -\dfrac{E(t_k)}{R_m} & 0 & 0 \\
0 & 0 & 0 & 0 & 0 \\
0 & 0 & 0 & 0 & 0
\end{bmatrix} \\
H_k &= \begin{bmatrix} -1/C_s & 0 & 0 & R_a & 0 \end{bmatrix}
\end{aligned}
\tag{3.7}
$$

3.1.3 Isovolumic expansion / contraction

The nonlinear functions $\boldsymbol{f}$, h, and the linearized matrices F and H_k for this stage are as follows.

$$
\begin{aligned}
\boldsymbol{f} &= \begin{bmatrix} -\dfrac{1}{R_{svr}}\left(\dfrac{V_s}{C_s} - \dfrac{V_r}{C_r}\right) + Q_{vad} \\ \dfrac{1}{R_{svr}}\left(\dfrac{V_s}{C_s} - \dfrac{V_r}{C_r}\right) \\ -Q_{vad} \\ \dot{Q}_{vad} \\ 0 \end{bmatrix} \\
h &= E(t_k)(V_{lv} - V_0) - (L_s\dot{Q}_{vad} + R_sQ_{vad} + V_s/C_s) \\
F &= \begin{bmatrix} -\dfrac{1}{C_sR_{svr}} & \dfrac{1}{C_rR_{svr}} & 0 & 0 & -\dfrac{1}{R_{svr}^2}\left(\dfrac{V_r}{C_r} - \dfrac{V_s}{C_s}\right) \\ \dfrac{1}{C_sR_{svr}} & -\dfrac{1}{C_rR_{svr}} & 0 & 0 & \dfrac{1}{R_{svr}^2}\left(\dfrac{V_r}{C_r} - \dfrac{V_s}{C_s}\right) \\ 0 & 0 & 0 & 0 & 0 \\ 0 & 0 & 0 & 0 & 0 \\ 0 & 0 & 0 & 0 & 0 \end{bmatrix} \\
H_k &= \begin{bmatrix} -1/C_s & 0 & 0 & R_a & 0 \end{bmatrix}
\end{aligned}
\tag{3.8}
$$

3.2 Process and Measurement Noise

Since the EKF operates on stochastic system models, we assume that the reduced order model is corrupted with process noise characterized by a zero mean Gaussian process with covariance $Q(t)$. In other words, the noise is assumed to be white Gaussian in nature. The same is true for measurement noise which is characterized by zero mean Gaussian process with covariance R_k. The overall performance of the EKF algorithm depends strongly on the

choice of these noise covariances. The measurement noise covariance is readily available from the specifications of the sensor that provides the data. In the case of the TORVAD^{TM}, the measurements of differential pressure are estimated by an embedded Kalman Filter [9], and have a noise of ± 5 mmHg. This information is used to set the measurement noise covariance as follows -

$$R_k(t) = 25$$

Ideally, the process noise covariance would be characterized by collecting sufficient data from the real process and performing statistical analysis. However, in the absence of such data, the process noise covariance $Q(t)$ needs to be tuned heuristically to give the best EKF performance. Some researchers have discussed a more methodical approach to deriving the EKF covariances, based on the normalization of the algorithm [4], however this approach is not used in this Thesis and is left as a possible step to be taken in the future. For the reduced order model, iterative and heuristic tuning results in the following process noise covariance -

$$Q(t) = \begin{bmatrix} 12 & 0 & 0 & 0 & 0 \\ 0 & 12 & 0 & 0 & 0 \\ 0 & 0 & 12 & 0 & 0 \\ 0 & 0 & 0 & 12 & 0 \\ 0 & 0 & 0 & 0 & 0 \end{bmatrix}$$

3.3 Initial Error Covariance

The EKF needs initial values of the states ($\boldsymbol{x}_0$) and the error covariance (P_0). The value of P_0 is indicative of the confidence we have in the initial state

$\boldsymbol{x}_0$. For the reduced order model, we are fairly certain of the initial conditions and the parameters. This allows us to simulate the EKF with different initial conditions, and test the limits of the algorithm. For the reduced order model, the algorithm is found to perform well with a standard deviation of around $\pm 30\%$ in the initial state and parameters.

3.4 Summary

This chapter discussed the Extended Kalman Filter, and how it can be used for parameter estimation. The equations for the filter were summarized, and the nonlinear functions ($\boldsymbol{f}$ and h) and linearized matrices (F and H_k) were presented for each stage of the cardiac cycle. Satisfactory performance of the EKF depends on careful tuning of the process noise covariance $Q(t)$ and measurement noise covariance $R_k(t)$. The process of selecting these covariance was discussed. Since we have reasonably good knowledge of the initial conditions for the reduced order model, we can change the initial covariance and states to test the EKF performance under varying initial uncertainty. The initial uncertainty for the best performance of the EKF was summarized.

The EKF algorithm, as described in this chapter, is used to run simulation tests for Chapter 5, and experimental tests for Chapter 6. The next chapter performs Identifiability and Estimability analysis on the EKF algorithm to gauge its ability to estimate states and SVR using the measurements available from the TORVAD$^{\text{TM}}$.

Chapter 4

Identifiability and Estimability

The ability to identify parameters by utilizing knowledge of the inputs and outputs of a system depends on the measurements available, and the model dynamics. If a change in the value of the parameters results in a detectable change in the output of the system, then those parameters are termed locally identifiable. A more formal treatment of this topic is presented in *Grewal et al.* [13].

Provided the parameters are identifiable, we can use a number of techniques to recover the parameter values with the available measurements. For this Thesis, the EKF algorithm is used to estimate both states and parameters of the reduced order model. For non-stochastic linear and non-linear observers, which can also estimate states and parameters albeit non-optimally, we have deterministic observability and controllability tests. These tests can reliably predict the stability and convergence of these estimators. However, it has been pointed out, that the same techniques might not apply to the case of stochastic systems [8]. There is a need to look into concepts of 'Stochastic observability' and 'Stochastic controllability'. An approach similar to the deterministic case of observability and contrallibility for stochastic linear systems is discussed in

Baram et al. [3], and is used to analyze the EKF used in this Thesis.

The following sections perform Identifiability analysis, and Estimability analysis to confirm the ability of the EKF algorithm presented in Chapter 3, to estimate states and SVR with the available measurements of differential pressure from the TORVAD^{TM}.

4.1 Identifiability Analysis

A linear system can consist of unknown, or uncertain parameters in its dynamic equations. If the value of the parameters are sufficiently known, drifts in their values over time are possible. For the CVS, the value of SVR can change over time, depending on cardiovascular health. If the deviated parameters result in an output that is distinguishable from the output generated for the old parameters, then the parameters are said to be locally identifiable [13]. Non linear systems can be linearized about an operating point, and if the outputs of this linearized system are distinguishable when the parameters change, then those parameters are locally identifiable as well [13]. For the latter case, not only is the linearized system locally identifiable, but so is the nonlinear system [13].

The reduced order model, as it is shown in Chapter 2 eqs. (2.9), (2.11) and (2.13), is linear time variant. As pointed out previously, the value of the left ventricle elastance, $E(t)$ is held constant between discreet time steps. If this simplification is made, then the system can be treated as time invariant between consecutive time steps. We can then use tests of identifiability on

a linear time invariant system as presented in [13], to find a minimum set of parameters, including R_{svr}, that are locally identifiable during each stage of the cardiac cycle using differential pressure as the measurement, and the VAD flow (Q_{vad}) as input.

For a linear time invariant system, the Markov parameter matrix is given by [13] :

$$G^T(\boldsymbol{\theta}) = \begin{bmatrix} D^T(\boldsymbol{\theta}) & (CB(\boldsymbol{\theta}))^T & (CAB(\boldsymbol{\theta}))^T & (CA^2B(\boldsymbol{\theta}))^T \dots & (CA^{2n-1}B(\boldsymbol{\theta}))^T \end{bmatrix} \tag{4.1}$$

The constant n in equation 4.1 represents the number of states. For the reduced order model, $n = 4$. The parameter vector $\boldsymbol{\theta}$ represents the unknown / uncertain parameters to be identified. The system matrices A, B, C and D can be obtained from the state equations shown in Chapter 2 eqs. (2.9), (2.11) and (2.13), and are summarized below.

4.1.1 Ejection

The linear matrices for this stage are summarized below.

$$A = \begin{bmatrix} -\frac{1}{C_s R_{svr}} & \frac{1}{C_r R_{svr}} & 0 & 1 \\ \frac{1}{C_s R_{svr}} & -\frac{1}{C_r R_{svr}} & 0 & 0 \\ 0 & 0 & 0 & -1 \\ -\frac{1}{C_s L_s} & 0 & \frac{E(t_k)}{L_s} & -\frac{R_a + R_s}{L_s} \end{bmatrix} \tag{4.2}$$

$$B = \begin{bmatrix} 0 & 0 & 0 & R_a/L_s \end{bmatrix}^T$$

$$C = \begin{bmatrix} 0 & 0 & 0 & R_a \end{bmatrix}$$

$$D = 0$$

4.1.2 Filling

The linear matrices for this stage are summarized below.

$$A = \begin{bmatrix} -\frac{1}{C_s R_{svr}} & \frac{1}{C_r R_{svr}} & 0 & 0 \\ \frac{1}{C_s R_{svr}} & -\frac{1}{C_r R_m} - \frac{1}{C_r R_{svr}} & \frac{E(t_k)}{R_m} & 0 \\ 0 & \frac{1}{C_r R_m} & -\frac{E(t_k)}{R_m} & 0 \\ 0 & 0 & 0 & 0 \end{bmatrix} \tag{4.3}$$

$$B = \begin{bmatrix} 1 & 0 & -1 & 0 \end{bmatrix}^T$$

$$C = \begin{bmatrix} -1/C_s & 0 & E(t_k) & 0 \end{bmatrix}$$

$$D = 0$$

4.1.3 Isovolumic expansion / contraction

The linear matrices for this stage are summarized below.

$$A = \begin{bmatrix} -\dfrac{1}{C_s R_{svr}} & \dfrac{1}{C_r R_{svr}} & 0 & 0 \\ \dfrac{1}{C_s R_{svr}} & -\dfrac{1}{C_r R_{svr}} & 0 & 0 \\ 0 & 0 & 0 & 0 \\ 0 & 0 & 0 & 0 \end{bmatrix} \tag{4.4}$$

$$B = \begin{bmatrix} 1 & 0 & -1 & 0 \end{bmatrix}^T$$

$$C = \begin{bmatrix} -1/C_s & 0 & E(t_k) & 0 \end{bmatrix}$$

$$D = 0$$

The parameters $\boldsymbol{\theta}$ are locally identifiable if the rank of the Jacobian of the Markov parameter matrix is equal to the number of parameters (q) to identify, i.e, the rank of the Jacobian is equal to the length of $\boldsymbol{\theta}$ [13]. This can be expressed mathematically as follows :

$$\text{rank}\left(\frac{\partial G^T(\boldsymbol{\theta})}{\partial \boldsymbol{\theta}}\right) = q \tag{4.5}$$

For the reduced order model, the following set of parameters is found to be locally identifiable, i.e equation (4.5) results in a rank of 4, for all stages of the cardiac cycle in presence of available measurements.

$$\boldsymbol{\theta} = \begin{bmatrix} R_{svr} & C_s & C_r & R_s \end{bmatrix}^T \tag{4.6}$$

It must be noted that the value of the left ventricle elastance, $E(t_k)$ is always nonzero because the last term, E_0 in equation (2.6) is nonzero for

the healthy and critical heart failure cases. If all the parameters shown above are identifiable, then R_{svr} is certainly identifiable if we assume reasonable knowledge of other parameters. Although this Thesis is only concerned with the estimation of SVR, a future extension of the work could include all of the parameters from equation (4.6) in the estimation algorithm.

4.2 Estimability Analysis

A system is said to be estimable, if when estimating its states from available measurement y_k ($k \geq$ no. of states n), the posterior error covariance is strictly smaller than the prior state covariance [3], i.e

$$E\left\{[\boldsymbol{x}(t) - \hat{\boldsymbol{x}}^+(t)][\boldsymbol{x}(t) - \hat{\boldsymbol{x}}^+(t)]^T\right\} < E\left\{[\boldsymbol{x}(t) - \hat{\boldsymbol{x}}^-(t)][\boldsymbol{x}(t) - \hat{\boldsymbol{x}}^-(t)]^T\right\} \tag{4.7}$$

After the k$^{\text{th}}$ measurement is done, the EKF algorithm (table 3.1) produces the k$^{\text{th}}$ estimate of states, $\hat{\boldsymbol{x}}^+(t)$. The error in estimating the true state can be written as :

$$\widetilde{\boldsymbol{x}} = \boldsymbol{x}(t) - \hat{\boldsymbol{x}}^+(t) \tag{4.8}$$

The covariance of this error, is then expressed as :

$$\begin{aligned} P_{\widetilde{\boldsymbol{x}}\widetilde{\boldsymbol{x}}} &= \Psi_{\widetilde{\boldsymbol{x}}\widetilde{\boldsymbol{x}}} + \boldsymbol{m}_{\widetilde{\boldsymbol{x}}}\boldsymbol{m}_{\widetilde{\boldsymbol{x}}}^T \\ &= E\left\{[\boldsymbol{x}(t) - \hat{\boldsymbol{x}}^+(t)][\boldsymbol{x}(t) - \hat{\boldsymbol{x}}^+(t)]^T\right\} + \boldsymbol{m}_{\widetilde{\boldsymbol{x}}}\boldsymbol{m}_{\widetilde{\boldsymbol{x}}}^T \end{aligned} \tag{4.9}$$

Since the EKF is an unbiased estimator [8], the last term in equation (4.9) goes to zero, i.e, $\boldsymbol{m}_{\widetilde{\boldsymbol{x}}} = 0$. We can then represent the error covariance as :

$$P_{\widetilde{\boldsymbol{x}}\widetilde{\boldsymbol{x}}} = E\left\{[\boldsymbol{x}(t) - \hat{\boldsymbol{x}}^+(t)][\boldsymbol{x}(t) - \hat{\boldsymbol{x}}^+(t)]^T\right\} \tag{4.10}$$

Before the k$^{\text{th}}$ measurement, the conditioned mean of the states is propagated using the system dynamics, and is represented by $\hat{\boldsymbol{x}}^-(t)$. The prior covariance of the states can then be written as :

$$P_{\hat{\boldsymbol{x}}^-\hat{\boldsymbol{x}}^-} = E\left\{[\boldsymbol{x}(t) - \hat{\boldsymbol{x}}^-(t)][\boldsymbol{x}(t) - \hat{\boldsymbol{x}}^-(t)]^T\right\} \tag{4.11}$$

We note that in the EKF equations of table 3.1, $P_{\tilde{\boldsymbol{x}}\tilde{\boldsymbol{x}}} = P_k^+$, and $P_{\hat{\boldsymbol{x}}^-\hat{\boldsymbol{x}}^-} = P_k^-$. Hence, we can rewrite equation (4.7) as :

$$P_k^+ < P_k^- \tag{4.12}$$

For the reduced order model, estimability can be analyzed by studying the results of the 'Error Covariance update' step. We shall test estimability of each state computationally, by running the EKF with the values of covariances and initial conditions discussed in Chapter 3. For each state, we will calculate 'δ', the difference between the posterior and prior covariance.

$$\delta = P_k^- - P_k^+ \tag{4.13}$$

The estimability for the state will be tested using this variable based on the following criteria :

$$\begin{aligned} &\delta > 0 \Rightarrow \text{State is estimable} \\ &\delta \leq 0 \Rightarrow \text{State is not estimable} \end{aligned} \tag{4.14}$$

The simulation is run for a continuous VAD flow of 5 L/min, and a healthy human. We find that the values of δ are always strictly greater than 0. To better visualize these values, they are plotted on a log scale against time (for $k \geq n$) for one cardiac cycle. The system states can be deemed

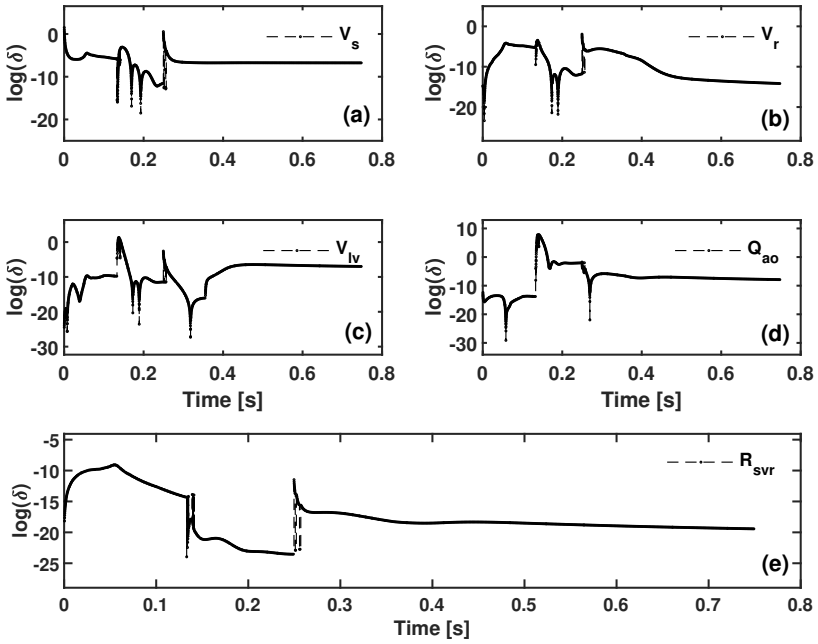

Figure 4.1: Value of $\log(\delta)$ of the covariance of (a)V_s (b)V_r (c)V_{lv} (d)Q_{ao} and (e)R_{svr}

estimable if their $\log(\delta)$ value exists ($\delta > 0$). Figure 4.1 shows these values for each state, and it is clear that the states are estimable in presence of available measurements from the TORVAD$^{\text{TM}}$.

The actual covariances of each state of the reduced order model, and SVR are shown in Figure 4.2. It is clear that the error covariance of SVR is driven down in each stage of the cardiac cycle, until it reaches a steady state value.

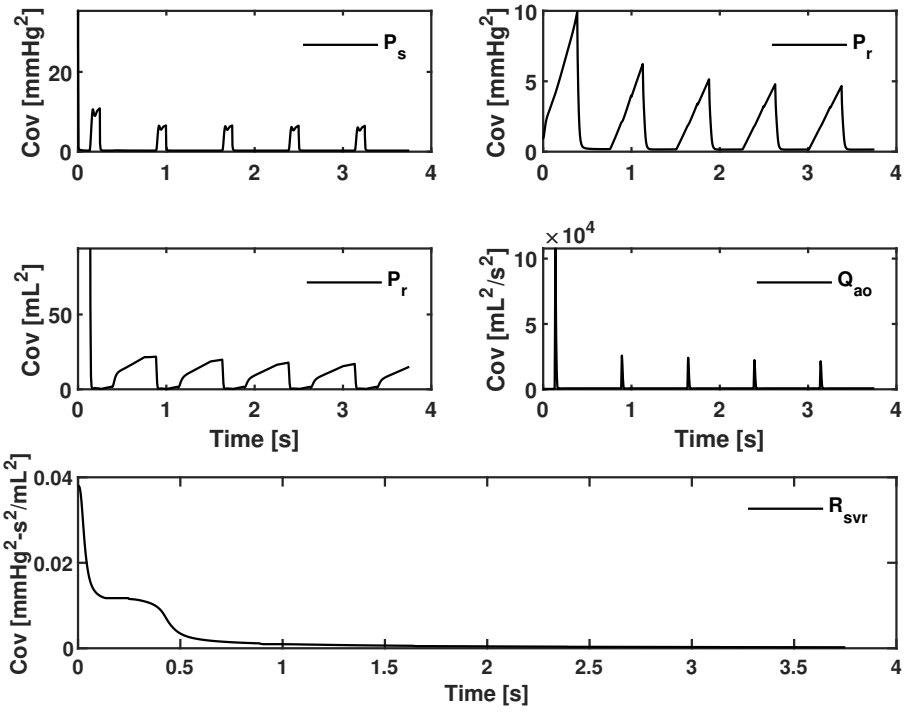

Figure 4.2: Covariances of each state and SVR for a typical simulation of the EKF algorithm.

4.3 Summary

This chapter focused on studying the EKF algorithm's ability to estimate the states, and SVR value of the CVS reduced order model. Through Identifiability analysis, it was shown that SVR, systemic circulation capacitance, pulmonary circulation capacitance and characteristic resistance of the aorta can all be identified from the output measurements of differential pressure. Estimability analysis was then done on the EKF algorithm to ensure that each measurement step brings down the error covariance, thereby helping

the algirhtm estimate states and SVR throughout the cardiac cycle.

The next two chapters will present results from simulation and experimental tests that demonstrate SVR estimation using the EKF algorithm. The tests will include results representative of healthy humans, and those with critical heart failure.

Chapter 5

Simulation Results

This chapter presents results from a simulation test of the EKF algorithm for SVR estimation as described in Chapter 3. Based on the Identifiability and Estimability analysis discussed in Chapter 4, we expect to be able to estimate SVR with the available measurements. The computational model was first simulated using Euler integration with a time step of 0.0001 s, and the values of parameters in the model were set to simulate a healthy and critical failure heart [11]. The value of each parameter is summarized in Appendix A. For the healthy case, the VAD flow rate was a constant, while for critical heart failure, pulsatile VAD flow was simulated using the following equation [11] :

$$Q_{vad} = \begin{cases} \dfrac{2\mathrm{SV}}{T_{ST}} \left(\dfrac{1}{2} - \dfrac{1}{2} \cos \left(\dfrac{2\pi(t_n - T_D)}{T_{ST}} \right) \right) & ; \text{if } T_D \leq t_n < T_D + T_{ST} \\ 0 & ; \text{Otherwise} \end{cases} \tag{5.1}$$

In the above equation, SV represents the stroke volume, and was set to 35 mL. T_{ST} is the ejection time for a complete stroke, and was set to 0.3 s. T_D is the time delay between the R wave, and the beginning of ejection. On the TORVAD$^{\mathrm{TM}}$, this parameter can be programmed to synchronize the start

of ejection to any point in the cardiac cycle. Its value was set to 0.24 s for both healthy and heart failure cases. t_n represents the normalized time, and is already described in Chapter 2 equation (2.4).

The differential pressure (ΔP) and VAD flow rate (Q_{vad}) at each time step during the simulation of the computational model were saved. Additive white Gaussian noise was then added offline, to simulate a 5% standard deviation in both the 'virtual sensor' readings. The noisy measurement data from simulating the computational model was then provided to the EKF algorithm. The reduced order model requires calculation of the derivative of VAD flow. The following section describes the calculation of this derivative.

The noisy measurement of VAD flow was first passed through a lowpass filter with the cutoff frequency set to one tenth of the sampling frequency. The filtered signal was then numerically differentiated, and smoothed using a moving average of 300 samples.

A block diagram representing the simulation of the algorithm is shown in Figure 5.1. For the healthy and heart failure cases, two tests were performed to gauge the performance of the algorithm. In the first test, the initial value of all states was shifted by some percentage 's' of their true value, as shown in the equation below.

$$\hat{\boldsymbol{x}}_{aug0} = \boldsymbol{x}_{aug0}\left(1 + \frac{s}{100}\right) \tag{5.2}$$

In the second test, the initial conditions were sampled from a Gaussian distribution with mean as the true value of each state, and a standard deviation

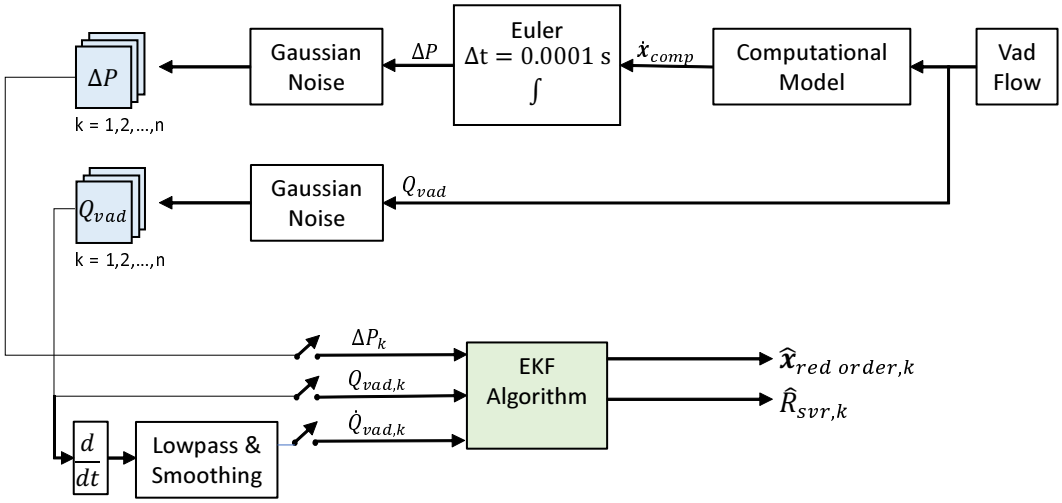

Figure 5.1: Block diagram of EKF algorithm simulation

of σ.

$$\hat{\boldsymbol{x}}_{aug,0} = \mathcal{N}(\boldsymbol{x}_{aug0}, \sigma^2) \tag{5.3}$$

Note that eqs. (5.2) and (5.3) both describe the initial conditions on the augmented state vector $\boldsymbol{x}_{aug}$ as described in equation (3.2). Within each test, the time it took for the R_{svr} estimate to settle within 2% of its final value was calculated as the '2% settling time'. The aboslute value of error was calculated using the following equation :

$$|\text{Error } \%| = 100\frac{\overline{\widehat{R}}_{svr} - R_{svr}}{R_{svr}} \tag{5.4}$$

Where $\overline{\widehat{R}}_{svr}$ represents the mean of the last 50 estimates of R_{svr}. The results from each test, as well as a figure showing the esitmates of all states and R_{svr} will be presented in the following sections. The initial value of the elements of the augmented state vector $\boldsymbol{x}_{aug}$ are summarized for each test in Appendix B.

5.1 Test with parameters set to a healthy heart

For this test, the parameters of the reduced order model were set as per table 2.4. The VAD flow rate was set to a constant value of 5 L/min. Figure 5.2 shows the measurements of Q_{vad} after addition of Gaussian white noise with mean 0 and covariance R_k as described in 3.2. It also shows the derivative, $\dot{Q}_{vad}$.

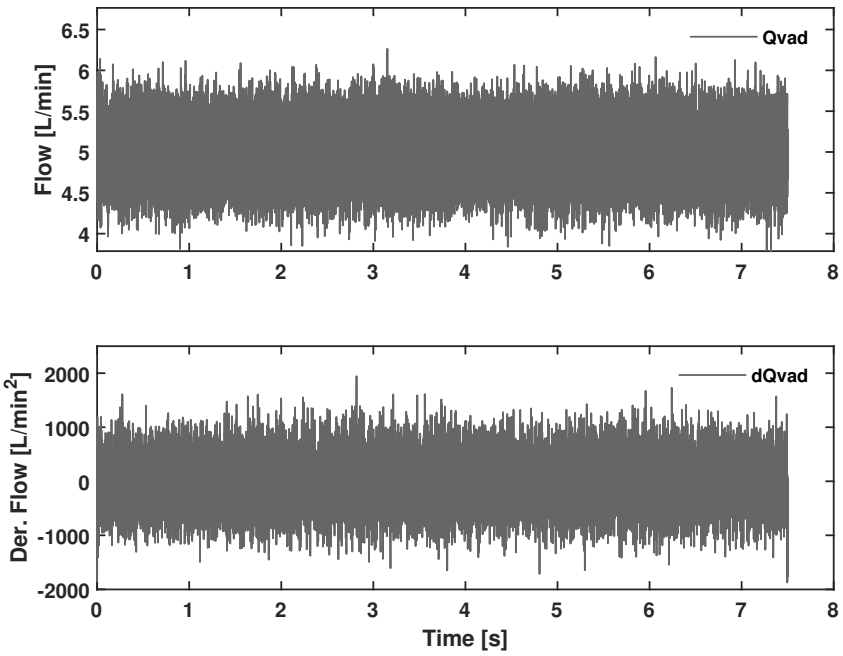

Figure 5.2: VAD Flow and derivative of VAD flow

5.1.1 Initial Conditions sampled from a Gaussian distribution

The results presented in table 5.1 convince us of the robustness of the algorithm, when the initial conditions are sampled from a Gaussian distribu-

tion with standard deviation as high as 50 units. The initial conditions are set according to equation (5.3). The EKF algorithm is able to estimate the value of R_{svr} within 1.75 % in all cases. The tests with the best and worst estimation accuracies are highlighted in green and brown respectively.

σ	| Error %|	2% Settling time (s)	Final Estimate
5	0.1015	3.36	0.9760
10	0.4201	1.8539	0.9791
20	1.3845	2.648	0.9885
30	1.7557	4.0891	0.9579
40	0.4690	3.1355	0.9704
50	1.2899	4.8817	0.9624

Table 5.1: Robustness test ICs sampled from a Gaussian distribution with standard deviation σ

Figure 5.3 shows R_{svr} estimates from a run with $\sigma = 30$ while figure 5.4 compares the estimated states and measurements with the computational model.

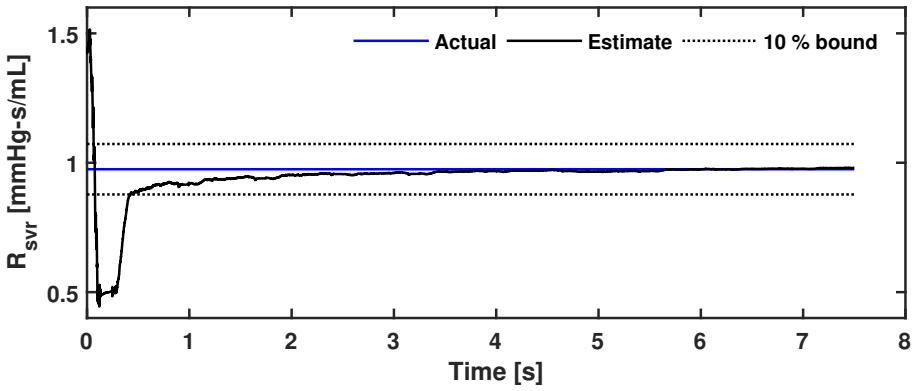

Figure 5.3: SVR Estimation for a healthy heart with $\sigma = 30$

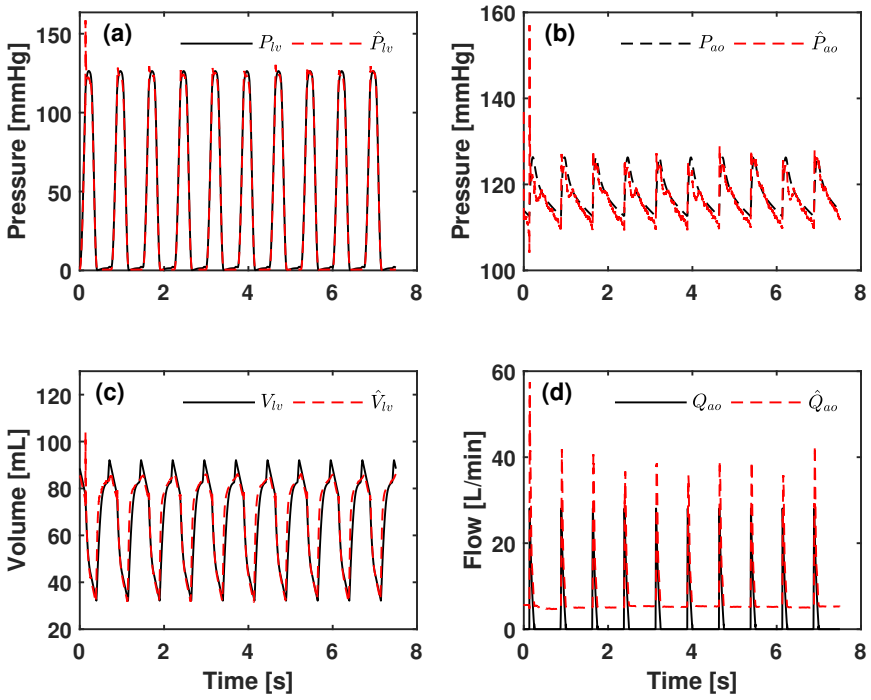

(a)

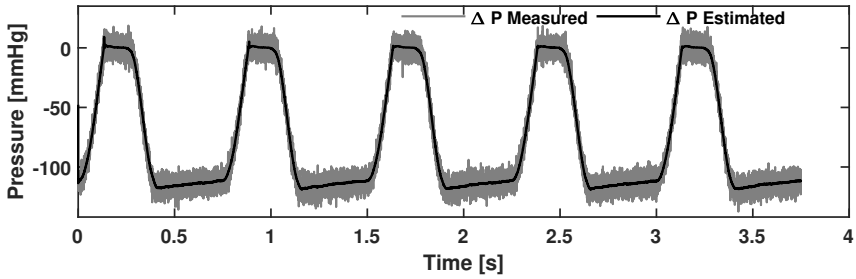

(b)

Figure 5.4: **a** Estimates of (a) LV pressure, (b) aortic pressure, (c) LV volume and (d) aortic flow for a healthy heart, $\sigma = 30$, **b** Estimated vs measured differential pressure for healthy person, ICs initialed with $\sigma = 30$

5.1.2 Initial Conditions shifted by some percentage of base value

Table 5.2 summarizes results from setting the initial conditions according to equation (5.2), with different values of s. For each of the cases, the EKF algorithm performs with an error % of 2 or below.

s(%)	| Error %|	2% Settling time (s)	Final Estimate
5	1.9974	1.1014	0.9945
10	0.1869	3.3490	0.9768
20	1.9665	4.6421	0.9558
30	0.0104	4.0951	0.9751
40	1.0455	3.8942	0.9648
50	0.3116	4.0737	0.9780

Table 5.2: Robustness test - ICs by s % of their base value

Figure 5.5 shows the SVR estimate for $s = 30$ %, and figure 5.6 shows the estimated states and measurements compared to the computational model.

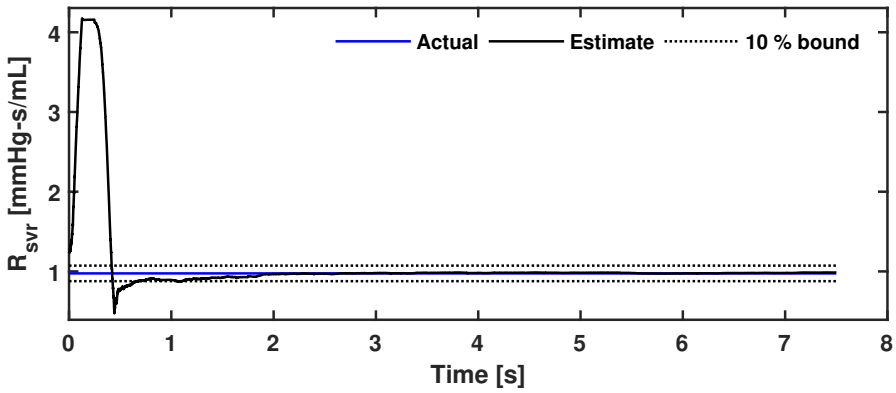

Figure 5.5: SVR Estimation for a healthy heart with s = 30 %

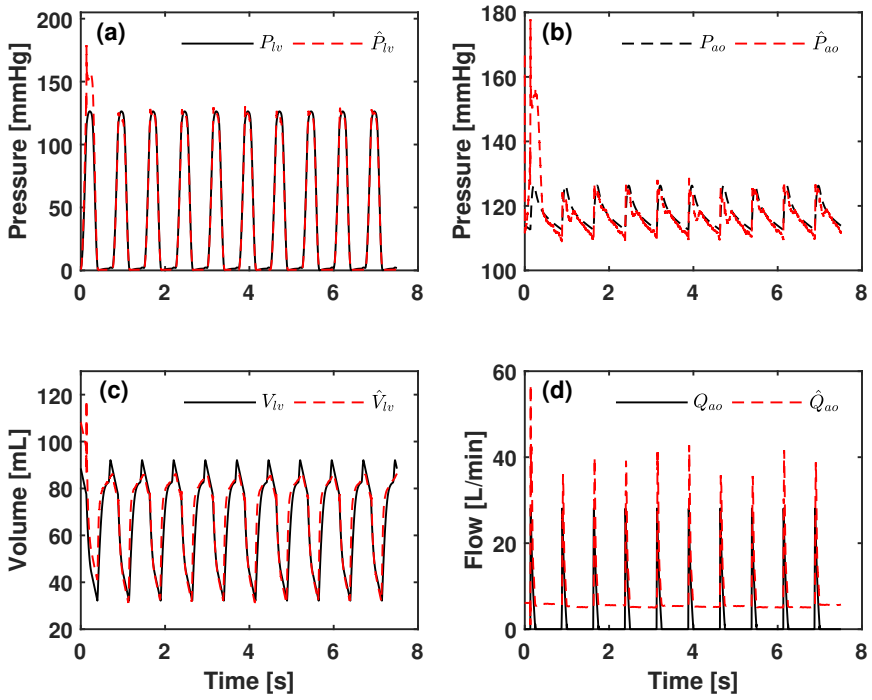

(a)

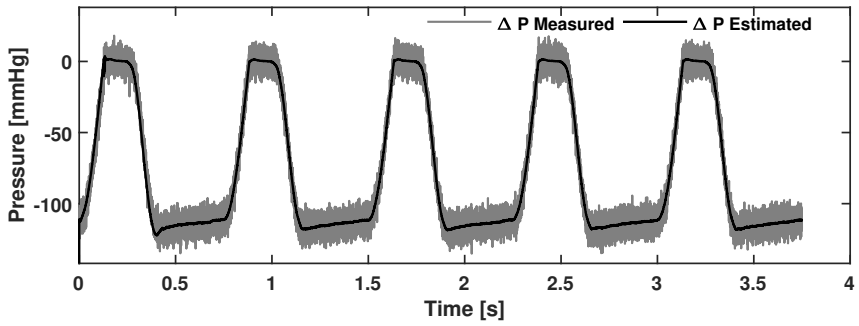

(b)

Figure 5.6: **a** Estimates of (a) LV pressure, (b) aortic pressure, (c) LV volume and (d) aortic flow for a healthy heart, $s = 30$ %, **b** Estimated vs measured differential pressure for healthy person, ICs shifted by $s = 30$ %

5.2 Test with parameters set to critical heart failure

For this test, the parameters of the reduced order model were set to the case of critical heart failure from table 2.4. The VAD flow rate was set to pulsatile, and was calculated using equation (5.1). Figure 5.7 shows the measurements of Q_{vad} after addition of zero mean Gaussian white noise with the same covariance as the previous section. The derivative, $\dot{Q}_{vad}$ is also shown.

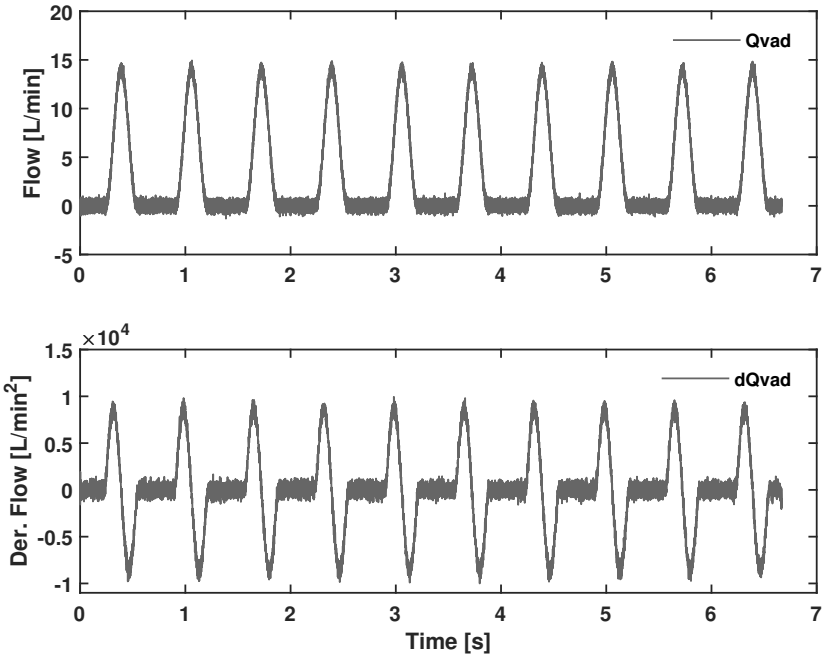

Figure 5.7: VAD flow and derivative of VAD flow used for EKF algorithm in critical heart failure simulation

5.2.1 Initial Conditions sampled from a Gaussian distribution

The results presented in table 5.3 demonstrate the robustness of the algorithm for the heart failure case, when the initial conditions are sampled from a Gaussian distribution with standard deviation as high as 40 units. The EKF is able to estimate the value of R_{svr} within 2.11 % in all cases.

$s(\%)$	| Error %|	2% Settling time (s)	Final Estimate
5	0.5646	6.3271	1.0640
10	0.0438	6.3546	1.0695
20	0.0764	6.3381	1.0692
30	2.1138	6.3832	1.0926
40	0.8861	6.3459	1.0605

Table 5.3: Robustness test - ICs sampled from a Gaussian distribution with standard deviation σ

Figure 5.8 shows R_{svr} estimates from a run with $\sigma = 30$ while figure 5.9 compares the estimated states and measurements with the computational model.

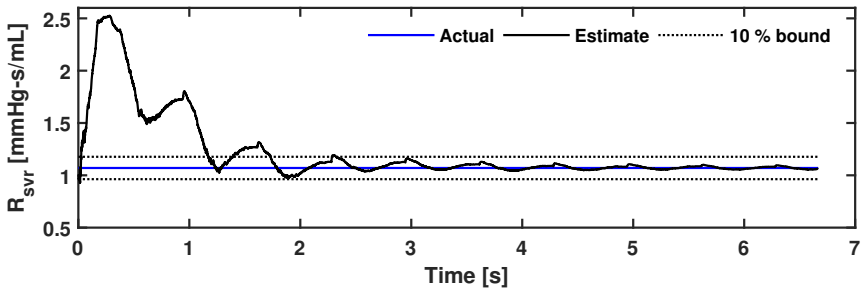

Figure 5.8: SVR Estimation for critical heart failure with $\sigma = 30$

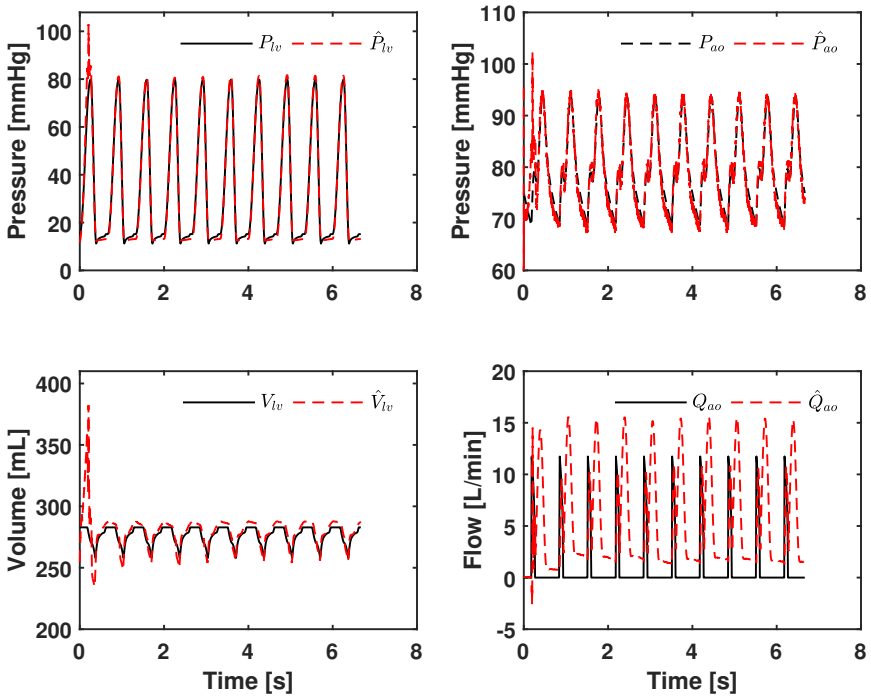

(a)

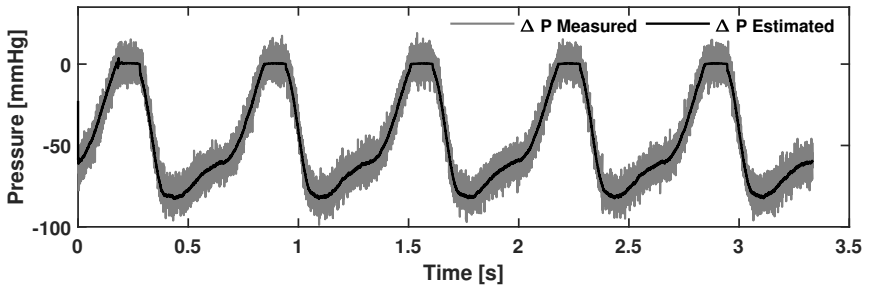

(b)

Figure 5.9: **a** Estimates of (a) LV pressure, (b) aortic pressure, (c) LV volume and (d) aortic flow for a healthy heart, $\sigma = 30$, **b** Estimated vs measured differential pressure for critical heart failure, ICs initialized randomly

5.2.2 Initial Conditions shifted by some percentage of base value

Table 5.4 summarizes results from setting the initial conditions according to equation (5.2), with different values of s. The EKF algorithm performs with a maximum error % of 2.21.

$s(\%)$	| Error %|	2% Settling time (s)	Final Estimate
5	0.0554	6.3301	1.0694
10	2.2140	6.3820	1.0937
20	1.7220	6.4094	1.0884
30	1.1629	6.4145	1.0576
40	1.7797	6.3695	1.0510

Table 5.4: Robustness test - ICs sampled from a Gaussian distribution with standard deviation σ

Figure 5.10 shows R_{svr} estimates from a run with $s = 30$ while figure 5.11 compares estimated states and measurements with the computational model.

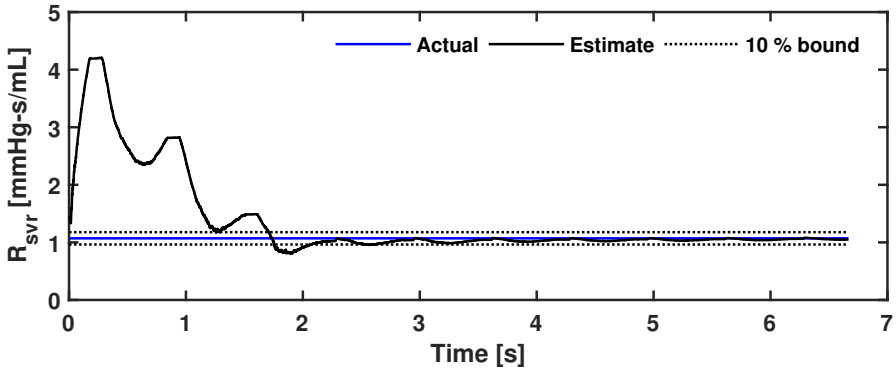

Figure 5.10: SVR Estimation for a healthy heart with $s = 30$

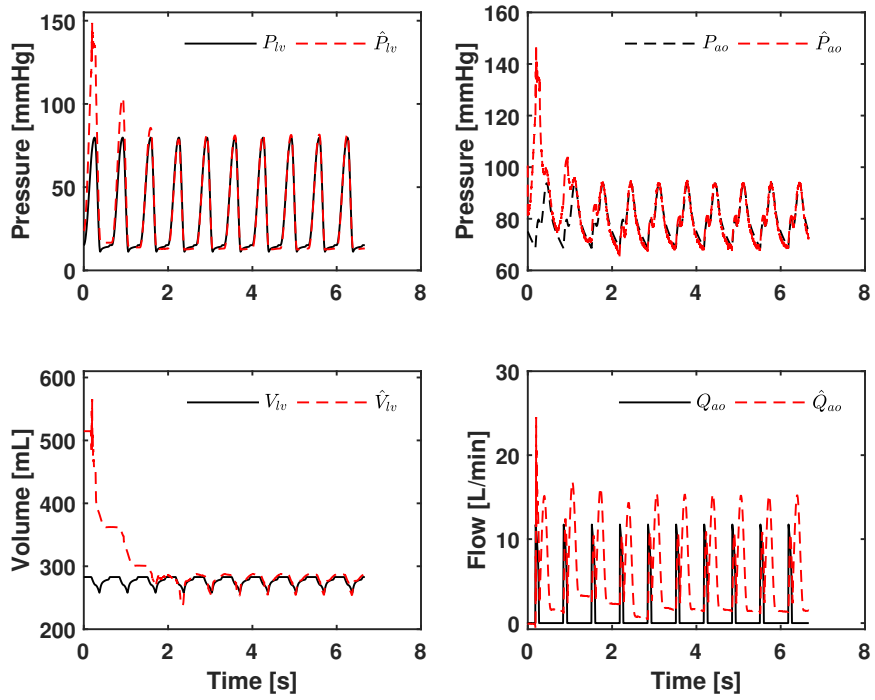

(a)

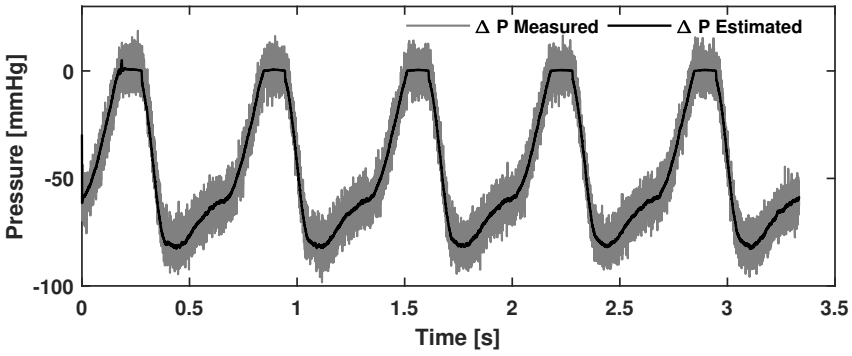

(b)

Figure 5.11: **a** Estimates of (a) LV pressure, (b) aortic pressure, (c) LV volume and (d) aortic flow for critical heart failure, $s = 30$, **b** Estimated vs measured differential pressure for healthy person, ICs initialed with $s = 30$

5.3 Summary

This chapter described simulation tests done on the EKF algorithm to prove robustness and accuracy. The computational model was run to generate 'virtual sensor' readings of VAD flow and differential pressure. These signals were then corrupted with additive Gaussian noise. Both healthy heart and critical heart failure was simulated. These measurements were then provided to the EKF algorithm, and the initial conditions and R_{svr} estimate was varied. The variation was either sampled from a Gaussian distribution, or was set to a fixed percentage from the base values. For the healthy heart case, the EKF algorithm was found to estimate R_{svr} an accuracy ranging between 0.0104 to 2 %. For this case, the algorithm converge for a wide range of initial conditions. For critical heart failure, the EKF algorithm was found to estimate R_{svr} with an accuracy ranging between 0.0438 to 2.21 %. For this case as well, the algorithm converged for a large range of initial conditions.

It must be noted that the successful convergence of the EKF algorithm relies on setting the heart rate accurately in the simulation. From the perspective of practical implementation, this information can be derived from the ECG signals that are available to the TORVAD^{TM}.

The next chapter will demonstrate SVR estimation using the EKF algorithm with measurement data collected from a mock circulation loop that is connected to the TORVAD^{TM}.

Chapter 6

Experimental Results

This chapter presents results of SVR estimation performed on data collected from the TORVAD^{TM} when connected to a mock circulation loop (MCL) which simulates the computational model. The MCL used for this experiment comprised of two chambers to emulate the left ventricle and aortic pressures, a re-circulation pump, and a flow interface to connect the LVAD. Such a setup allows us to operate the TORVAD^{TM} in an emulated cardiovascular environment that is as close as possible to reality. The control loop in the MCL, along with its parameters, can be tuned to emulate different heart conditions. For the experiment presented in this Chapter, conditions for critical heart failure were emulated. All the data used for this test was provided by Windmill Cardiovascular Systems In. (Austin, TX). This chapter is organized into five sections. The first section describes the collection of data from the TORVAD^{TM}, and the processing done on it before using it for the estimation algorithm. The second section discusses the selection of initial conditions for the states and R_{svr} used for the EKF algorithm. A description of the initial values of the error covariance matrix is also given. The third section shows results of SVR estimation from the experiment. The fourth section shows the robustness of the algorithm to different initial values of SVR. The last section

summarizes the experiment and results discussed in this chapter.

6.1 Description of the Experiment

As discussed earlier, the TORVAD^{TM} has the capability to estimate differential pressure and VAD flow using embedded Kalman Filters [9], and can log the data to a computer at a rate of 450 Hz. An experiment was performed and the data collected from the TORVAD^{TM} was interpolated using 1-D linear interpolation to emulate a sampling rate of 10 kHz. The interpolated differential pressure (ΔP) was used as a measurement for the EKF algorithm, and the VAD flow rate (Q_{vad}) was used as an input. The same low pass filtering and smoothing as described in Chapter 5, was applied to numerically differentiate VAD flow rate to obtain $\dot{Q}_{vad}$.

Figure 6.1 shows a block diagram describing collection of data from the TORVAD^{TM}, and the EKF algorithm for estimating SVR. In the figure, 'VC' represents the voice coils used as actuators to drive pressure in the chambers, 'LV' is the left ventricle chamber, 'AO' is the aortic chamber, 'BP' is the blood re-circulation pump, and 'TORVAD' represents the LVAD device.

During the experiment, the TORVAD^{TM} was programmed to operate in synchronous counter-pulse mode. The mean VAD flow rate recorded was 2.24 L/min. The interpolated VAD flow, and the derivative of VAD flow ($\dot{Q}_{vad}$), computed numerically is shown in Figure 6.2. The value of maximum and minimum left ventricle elastance were set to 0.5 and 0.0466 mL/mmHg respectively.

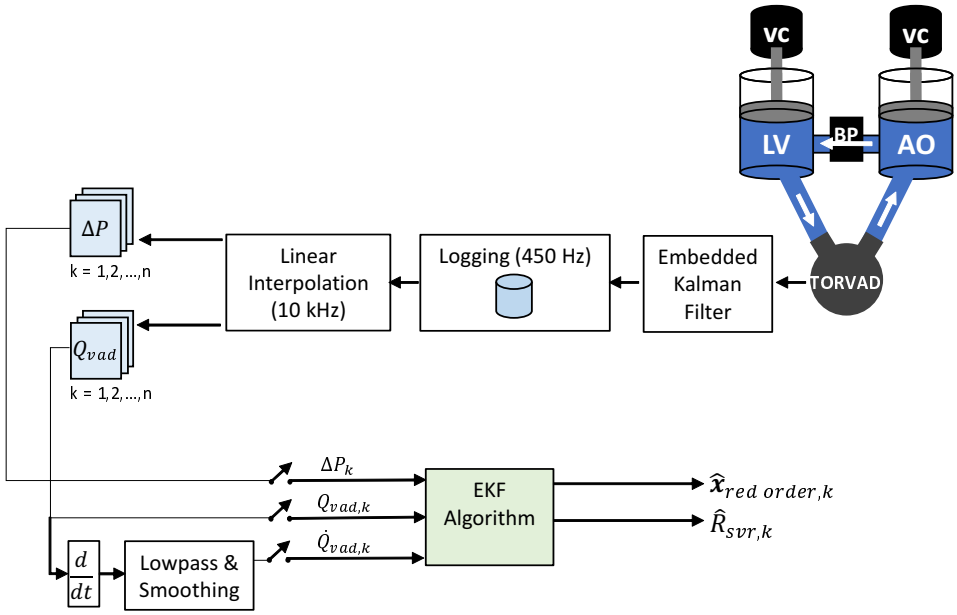

Figure 6.1: Block diagram of the SVR estimation experiment. TORVAD connected to MCL logs data to a computer. Data is sent to EKF algorithm after interpolation.

6.2 Initial Conditions

Table 6.1 summarizes the initial conditions used for the states, and R_{svr} while running the EKF algorithm. The actual value of R_{svr} used in the MCL was 1.05 mmHg-s/mL, and the final estimate of the algorithm was compared against this value. Since the MCL simulates the computational model, and we can only approximately calculate the initial conditions of the reduced order model from the initial conditions of the computational model, the values summarized here are an informed guess at best. For this reason, the initial error covariance has some uncertainty corresponding to the value of the initial state estimates.

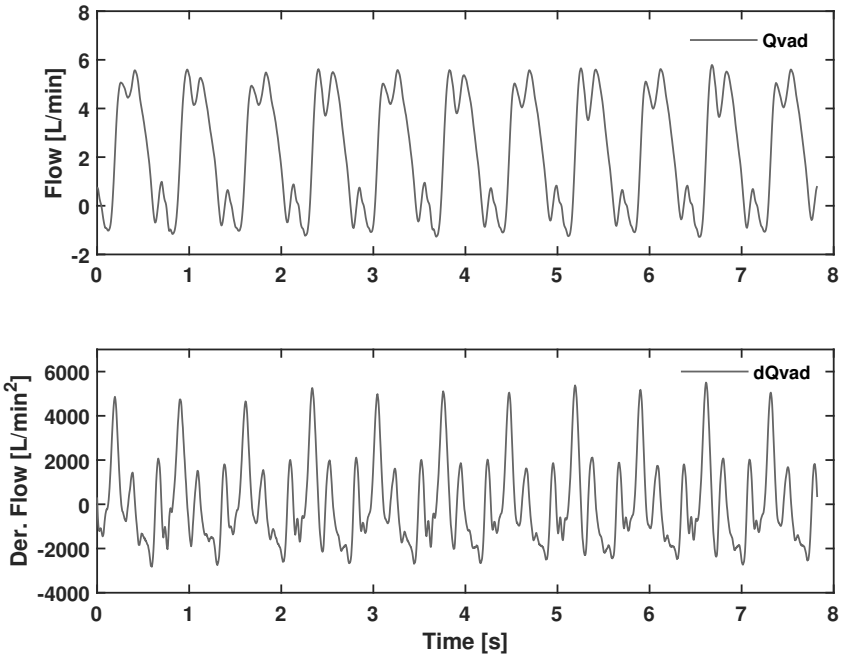

Figure 6.2: VAD Flow and derivative of VAD flow.

We assume that the initial states and SVR are deviated by 10 % of their true value. The initial error covariance (P_0) obtained using this assumption is as follows :

$$P_0 = \begin{bmatrix} 148.7 & 0 & 0 & 0 & 0 \\ 0 & 409 & 0 & 0 & 0 \\ 0 & 0 & 8100 & 0 & 0 \\ 0 & 0 & 0 & 0 & 0 \\ 0 & 0 & 0 & 0 & 0.011 \end{bmatrix} \tag{6.1}$$

It is clear from the above equation that the highest uncertainty is placed on the initial value of V_{lv} and V_r. The value of the process noise covariance was

State	Initial Value	Units
V_s	40.6480	mL
V_r	67.4150	mL
V_{lv}	300	mL
Q_{ao}	0	mL/s
R_{svr}	1.1603	mHg-s/mL

Table 6.1: Initial value of the augmented states for the EKF algorithm

the same as that set for the simulation tests described in Chapter 5.

$$Q_k = \begin{bmatrix} 12 & 0 & 0 & 0 & 0 \\ 0 & 12 & 0 & 0 & 0 \\ 0 & 0 & 12 & 0 & 0 \\ 0 & 0 & 0 & 12 & 0 \\ 0 & 0 & 0 & 0 & 0 \end{bmatrix} \tag{6.2}$$

6.3 Results

For the initial conditions, error covariance and process noise covariance set to values described in the previous section, the EKF algorithm achieved an accuracy of 0.3614 %. SVR estimates were able to settle to 2% of their final value in a span of 7.48 seconds. The estimated SVR was 1.0538 mmHg-s/mL. Figure 6.3 shows results of SVR estimation.

Figure 6.4 shows the estimated pressures in the left ventricle, aorta and left atrium from the last 5 cardiac cycles. It also shows a comparison between the measured and estimated differential pressure. The aortic flow and left ventricle volume estimated by the EKF algorithm is shown for the last 5 cardiac cycles in Figure 6.5.

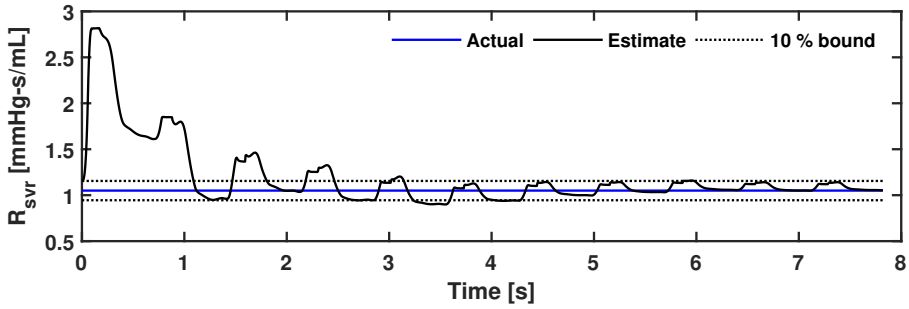

Figure 6.3: SVR estimation using measurements obtained from the TORVAD, which was connected to a MCL.

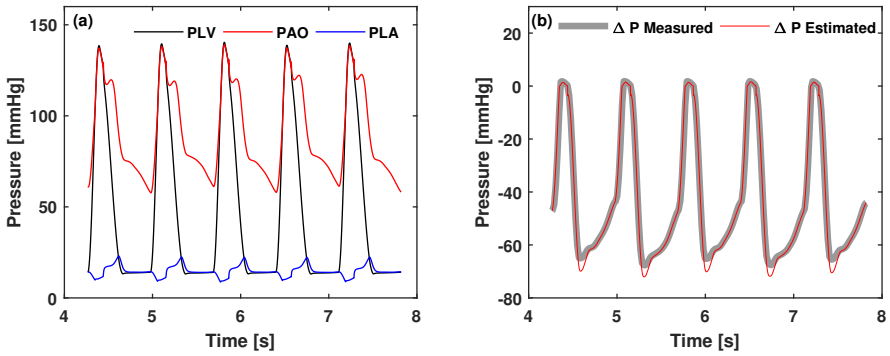

Figure 6.4: (a) Estimated pressures in the left ventricle, aorta and left atria. (b) Comparison of measured and estimated differential pressure.

6.4 Robustness under different initial conditions

To test the robustness of the algorithm, the initial value of SVR was deviated from its true value. Two types of tests were performed. In both the tests, the uncertainty in the initial value of states of the reduced order model was kept same. The nature of these tests was the same as described in Chapter 5. In the first test, initial SVR was deviated by a some percentage s of its true value. In the second test, initial SVR was sampled from a Gaussian

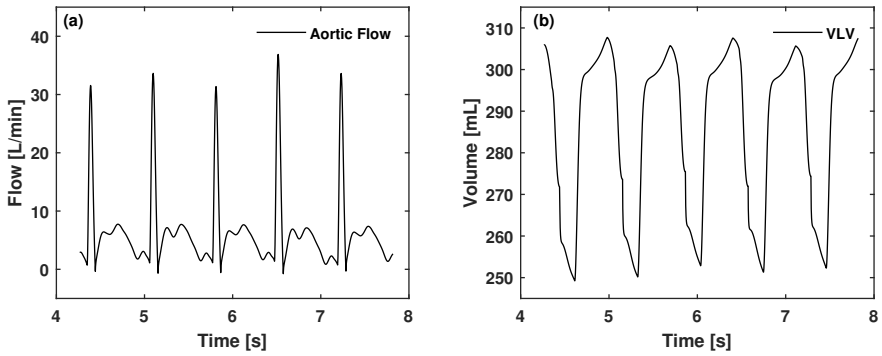

Figure 6.5: (a). Aortic flow estimated by the EKF algorithm. (b) Left ventricle volume estimated by the EKF algorithm.

distribution with mean equal to the true value of SVR set in the MCL, and a standard deviation of σ.

6.4.1 SVR initialized with some percent shift

The results from this test are summarized in table 6.2. The algorithm was able to estimate SVR with a best case accuracy of 0.3614 % for $s = 10$ %, and worst case accuracy of 6.4345 % for $s = 50$ %. The SVR estimation results shown in section 6.3 in Figure 6.3 are for the case of $s = 10$ %.

$s_{svr}(\%)$	| Error %|	2% Settling time (s)	Final Estimate
5	3.7029	7.4880	1.0889
10	0.3614	7.4891	1.0538
20	1.7314	7.4830	1.0318
40	4.7846	7.4734	0.9998
50	6.4345	7.4686	0.9824

Table 6.2: Robustness test - initial R_{svr} deviated a fixed percentage s from its true value.

6.4.2 SVR initialized from a Gaussian distribution

The results from this test are summarized in table 6.3. The algorithm was able to estimate SVR with a best case accuracy of 3.0790 % for $\sigma = 20$, and worst case accuracy of 5.4124 % for $\sigma = 50$. Figure 6.6 shows SVR estimates

σ_{svr}	| Error %|	2% Settling time (s)	Final Estimate
5	3.7415	7.4879	1.0893
10	2.3959	7.4952	1.0752
20	3.0790	7.4981	1.0823
30	5.1409	7.5001	1.1040
40	5.2915	7.4718	0.9944
50	5.4124	7.4715	0.9932

Table 6.3: Robustness test - initial R_{svr} sampled from a Gaussian distribution with standard deviation σ and mean as true R_{svr}.

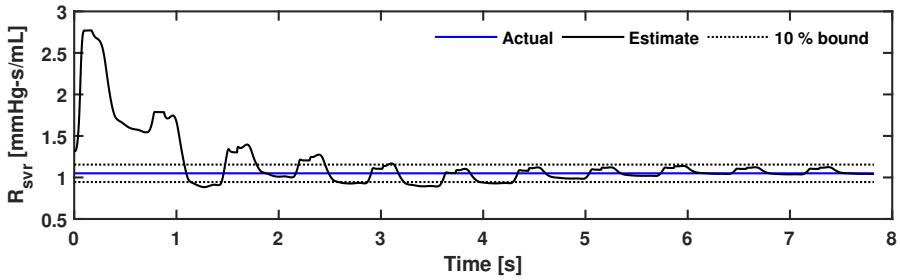

Figure 6.6: SVR Estimation for $\sigma = 10$

from a typical ensemble with $\sigma_{svr} = 10$. Figure 6.7 shows the estimated pressures in the left ventricle, aorta and left atria for the last 5 cycles, while Figure 6.8 shows the estimated aortic flow and left ventricle volume.

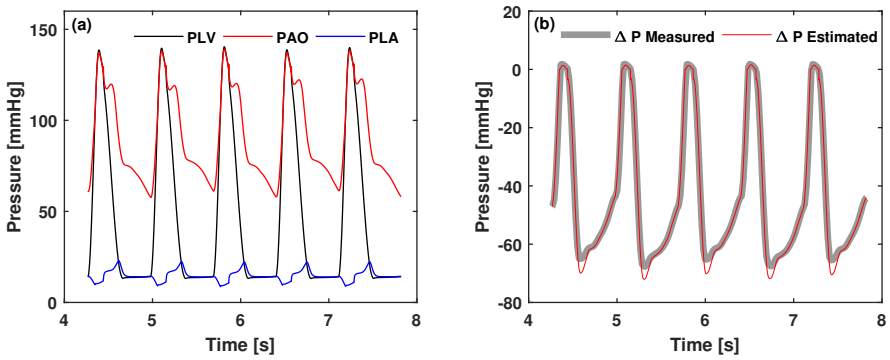

Figure 6.7: (a) Estimated pressures in the left ventricle, aorta and left atria, (b) Comparison of measured and estimated differential pressure for $\sigma = 10$

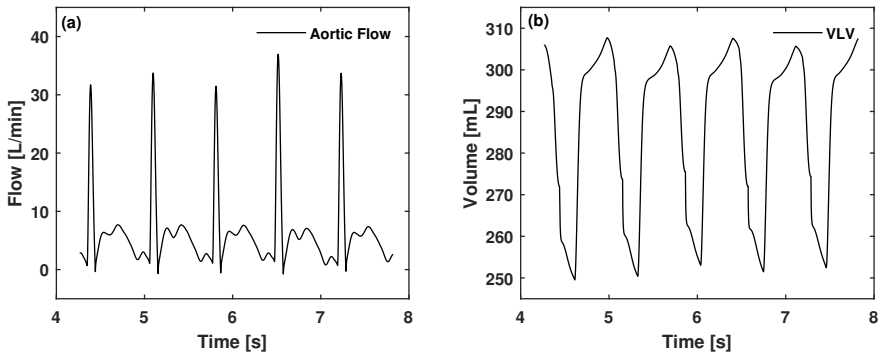

Figure 6.8: (a) Estimated aortic flow, (b) Estimated left ventricle volume for $\sigma = 10$

6.5 Summary

This chapter described an experiment where SVR estimation was done using data collected from the TORVAD^{TM} while it was connected to a mock circulation loop. The MCL was tuned to simulate conditions for critical heart failure, and the embedded Kalman Filter of the TORVAD^{TM} logged the esti-

mates of differential pressure and VAD flow to a computer at the rate of 450 Hz. This data was then interpolated to a rate of 10 kHz and used in the EKF algorithm described in Chapter 3.

The initial condition for the states of the reduced order model were kept fixed during all tests, while the initial value of SVR was deviated from its true value to test the robustness of the algorithm. Two types of tests were performed - in the first test, the initial value of SVR was shifted from its true value by some percent s, and in the second test it was sampled from a Gaussian distribution with mean equal to the true value, and standard deviation of σ. The algorithm was found to converge, and estimated SVR with an overall best case accuracy of 0.3614 % ($s = 10$), and a worst case accuracy of 6.4345 % ($s = 50$). The results demonstrate the satisfactory performance of the estimation algorithm when applied to experimental data collected from the TORVAD$^{\text{TM}}$.

This chapter marks the end of this Thesis. The next chapter concludes and summarizes the Thesis, and discusses future work that can be done to improve SVR estimation, or extended it for higher level control of the TORVAD$^{\text{TM}}$.

Chapter 7

Conclusions and Future Work

7.1 Conclusions

Systemic Vascular Resistance (SVR) is the aggregate resistance to blood flow faced by the left ventricle during ejection. The primary goal of this Thesis was to investigate methods of recursively estimating SVR, using measurements provided by an implantable rotary left ventricular assist device, the TORVAD^{TM} (Windmill Cardiovascular Systems In., Austin, TX). The ability to estimate this parameter recursively could pave the way for embedded real-time estimation of SVR. Tracking the trends of SVR over time can help catch abnormalities in the physiology of the cardiovascular system of a person, thereby helping diagnose disease and in some cases predict mortality [24, 30, 5, 2]. An Extended Kalman Filter (EKF) was used in this Thesis to estimate SVR by using differential pressure (ΔP) as measurements and VAD flow rate (Q_{vad}) as a known input. This approach is similar to the one taken in *Yu et al.* [31]. The EKF algorithm uses a model to propagate the conditional mean and error covariance of the model states forward in time, and uses measurements to update both these values. The updated conditional mean (conditioned on the latest measurement) can then be treated as the 'most likely' estimate of the states, while the error covariance represents the

confidence we can place on these estimates.

The first part of this Thesis, comprising of Chapters 2 and 3, focused on modeling of the cardiovascular system, and developing the EKF algorithm. Chapter 2 focused on introducing two models - the computational model, and the reduced order model. The reduced order model contains 4 states, and was used to design the EKF algorithm, while the computational model contains 12 states, and was used to generate 'simulated sensor measurements' of ΔP and Q_{vad}. The design of the EKF algorithm was discussed in Chapter 3.

The second part of the Thesis, consisting of Chapter 4, focused on performing Identifiability analysis on the reduced order model, and Estimability analysis on the EKF algorithm designed in Chapter 3. According to *Grewal et al.* [13], a set of parameters of a dynamic system are identifiable if, a change in their values results in a distinguishable change in the outputs. For the reduced order model, if we were to treat the VAD flow rate as input, and differential pressure as output, then the SVR (R_{svr}), systemic circulation compliance (C_s), pulmonary circulation compliance (C_r) and characteristic aortic resistance (R_c) are all identifiable. This Thesis focussed on SVR alone. For deterministic dynamic systems, the ability to reconstruct system states from output measurements can be gauged by studying its observability. For stochastic systems, the ability to estimate states by using avaiable measurements must be gauged by using stochastic observability [8]. According to *Baram et al.*, 'estimability' can hold as a good test of stochastic observability, and this test is performed for the EKF algorithm designed for the reduced order model. We

find that the system states (including SVR) are estimable.

The third and final part of the Thesis, comprising of Chapters 5 and 6, focused on testing the accuracy of SVR estimation using the EKF algorithm. Chapter 5 presented results of simulations where the measurements were generated by simulating the computational model, and the measurements were corrupted by additive Gaussian white noise. The tests were run for a healthy heart, and for critical heart failure. Within each case, tests were performed where initial conditions were either shifted by a percentage of their true value, or were sampled randomly from a Guassian distribution. Chapter 6 presented experimental results for SVR estimation. The measurements were collected from the TORVAD$^{\text{TM}}$, which was connected to a mock circulation loop. The MCL was propgrammed to emulate critical heart failure. These measurements were then fed to a simulation of the EKF algorithm. For this chapter as well, tests were done where the initial SVR value was either deviated by a percentage of its true value, or sampled from a Gaussian distribution. Table 7.1 summarizes the accuracy of the algorithm for all cases.

Test	**Best case Accuracy (%)**	**Worst case Accuracy (%)**
Healthy (Simulation)	0.0104	1.9974
Critical HF (Simulation)	0.0438	2.2140
Critical HF (Experiment)	0.3614	6.4345

Table 7.1: Summary of EKF algorithm accuracy

7.2 Future Work

The EKF algorithm designed in this Thesis estimates the states of the reduced order model, along with SVR. However, identifiability analysis performed in Chapter 4 revealed that parameters other than SVR could possibly be identified by using differential pressure as an output measurement, and VAD flow rate as the input. If an EKF algorithm was designed to estimate these parameters as well, estimability analysis on such an algorithm could be done in the future to study the feasibility and accuracy in estimating each parameter.

The inclusion of SVR to augment the state vector for the reducecd order model makes the system nonlinear, and this motivates the use of the EKF for estimation. In recent years, the Unscented Kalman Filter (UKF) has been developed for nonlinear systems and has been found to perform better than the EKF in some cases [27]. A comparison of the accuracy of SVR estimation between the EKF and UKF could be done in the future.

The EKF algorithm discussed in this Thesis was simulated on the commercial software MATLAB Release 2018b (The MathWorks, Inc., Natick, Massachusetts, United States). If the algorithm must run on an embedded microcontroller or a real-time environment, it must be modified slightly and tested for numerical stability. For instance, the microcontroller might not be capable of data acquisition at the rate of 10 kHz, which was the rate used during simulations. An emulation study with slower sampling rates could be done in simulations to test the algorithm. It is also common for micro-controllers

to use fixed point algebra, as opposed to floating point algebra used by the processors in modern computers. The dynamic equations shows in this Thesis could be discretized, and adapted for fixed point algebra for this purpose. Such an approach has been taken by *Dhaouadi et al.* for EKF based state estimation of a permanent magnet synchronous motor [7].

Finally, a possible extension of the work presented in this Thesis could be utilization of SVR estimates for higher level physiological control of the TORVAD^{TM}, remote diagnostics and event based alarming. Figure 7.1 shows a block diagram of the possible ways of utilizing SVR estimates.

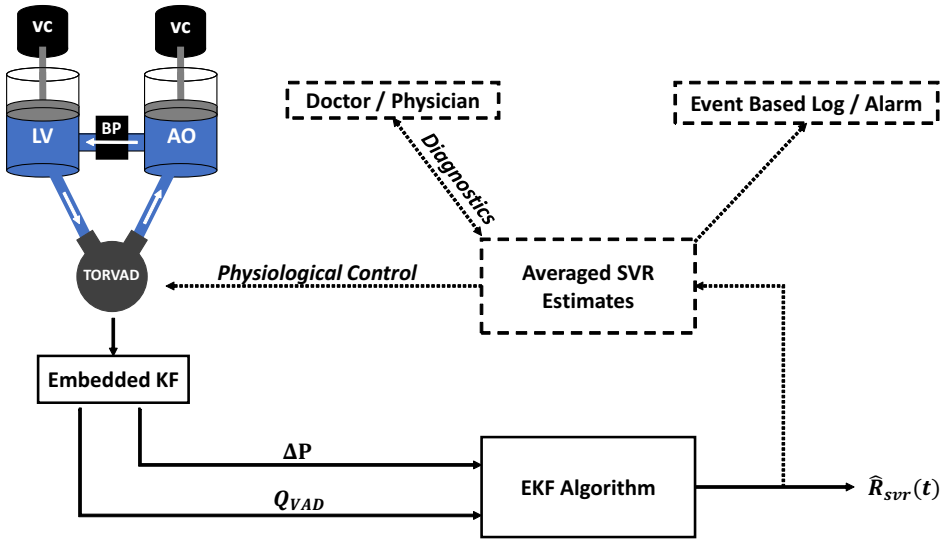

Figure 7.1: Physiological Control, remote diagnostics and event based alarming through real-time SVR estimation.

7.3 Summary

This Thesis developed an EKF algorithm based on a reduced order model of the cardiovascular system for the purpose of estimating Systemic Vascular Resistance by using measurements from a left ventricular assist device. The algorithm enables recursive estimation, and hence is well suited for adapting to real-time application on an embedded micro-controller. The parameters of the reduced order model were tuned by matching the impedance of the systemic circulation circuit with that of a higher order computational model. Identifiability and Estimability analysis was performed on the algorithm to ensure that we could estimate SVR by using the measurements available from the LVAD. Tests were performed for a healthy heart and a critical heart. In simulation tests, the measurements were generating by simulating the computational model, and adding additive Gaussian White noise to the measurements. An experiment was also performed where measurements were taken from the TORVAD^{TM} when it was connected to an MCL. Finally, possible work and extensions of the work done in this Thesis were discussed. These included estimating more parameters, comparison with the UKF algorithm, discretization for implementation on a micro-controller and utilizing SVR estimates for higher level control and diagnostics.

Appendices

Appendix A

Values of elements of computational model

The following table summarizes the values of each parameter of the computational model.

Parameter	**Description**	**Value**	**Units**
R_t	Valve resistance	0.0025	mmHg-s/mL
E_{max}	Maximum left ventricle elastance	3.25 (0.30)	mmHg/mL
E_0	Minimum left ventricle elastance	0.0068 (0.046)	mmHg/mL
V_0	Unstressed volume in left ventricle	5	mL
R_{sa}	Systemic artery resistance	0.15	mmHg-s/mL
C_{sa}	Systemic artery compliance	1.25 (0.65)	mL/mmHg
L_{sa}	Systemic artery inertance	0.0022	mmHg-s^2/mL
R_{st}	Systemic arterial tree resistance	0.8 (0.9)	mmHg-s/mL
C_{st}	Systemic arterial tree compliance	2.0 (1.5)	mL/mmHg
R_{sv}	Systemic venous resistance	0.025	mmHg-s/mL
C_{sv}	Systemic venous compliance	20	mL/mmHg
R_{pa}	Pulmonary aratery resistance	0.07	mmHg-s/mL
C_{pa}	Pulmonary artery compliance	7.5	mL/mmHg
L_{pa}	Pulmonary artery inertia	0.0018	mmHg-s^2/mL
R_{pt}	Pulmonary arterial tree resistance	0.04	mmHg-s/mL
C_{pt}	Pulmonary arterial tree compliance	0.5	mL/mmHg
R_{pv}	Pulmonary venous resistance	0.003	mmHg-s/mL
C_{pv}	Pulmonary venous compliance	20	mL/mmHg

Table A.1: Parameters used in the computational model. Values in paranthesis represent conditions for heart failure.

Appendix B

Initial Conditions for the reduced order model

B.1 Simulation without VAD support

The initial conditions for the reduced order model when simulating healthy heart conditions without VAD support are summarized below.

State	Initial Value	Units
V_s	148.2756	mL
V_r	4.9841	mL
V_{lv}	88.6363	mL
Q_{ao}	83.2676	mL/s

Table B.1: Initial values of the reduced order model for healthy heart conditions and no VAD support

The initial conditions for the reduced order model when simulating critical heart failure conditions without VAD support are summarized below.

State	Initial Value	Units
V_s	32.4040	mL
V_r	59.8169	mL
V_{lv}	293.6323	mL
Q_{ao}	-0.4611	mL/s

Table B.2: Initial values of the reduced order model for critical heart failure and no VAD support

B.2 Estimation using simulated measurements

The initial conditions used for simulation test for a healthy heart described in Chapter 5 are summarized below.

State	Initial Value	Units
V_s	146.2351	mL
V_r	4.8887	mL
V_{lv}	86.5762	mL
Q_{ao}	83.1969	mL/s
R_{svr}	0.975	mmHg-s/mL

Table B.3: Initial values of the reduced order model for healthy heart simulation test

THe initial conditions used for simulation test for critical heart failure conditions in Chapter 5 are summarized below.

State	Initial Value	Units
V_s	55.9645	mL
V_r	57.6267	mL
V_{lv}	279.8088	mL
Q_{ao}	-0.5161	mL/s
R_{svr}	1.07	mmHg-s/mL

Table B.4: Initial values of the reduced order model for critical heart failure simulation test

Bibliography

[1] Amr E. Abbas, F. David Fortuin, Bhavesh Patel, Carlos A. Moreno, Nelson B. Schiller, and Steven J. Lester. Noninvasive measurement of systemic vascular resistance using Doppler echocardiography. *Journal of the American Society of Echocardiography*, 17(8):834–838, 2004.

[2] Yusuke Abe, Tsuneo Chinzei, Kunihiko Mabuchi, AJ Snyder, Takashi Isoyama, K Imanishi, T Yonezawa, Hiroyuki Matsuura, Akimasa Kouno, Toshiya Ono, Kazuhiko Atsumi, Iwao Fujimasa, and Kou Imachi. Physiological control of a total artificial heart: conductance- and arterial pressure-based control. *Journal of Applied Physiology*, 1998.

[3] Yoram Baram and Thomas Kailath. Estimability and Regulability of Linear Systems. *IEEE Transactions on Automatic Control*, 33(12):1116–1121, 1988.

[4] S Bolognani, L Tubiana, and M Zigliotto. Extended Kalman filter tuning in sensorless PMSM drives. *IEEE Transactions on Industry Applications*, 39(6):1741–1747, 2003.

[5] J R Boston, Marwan A Simaan, James F Antaki, and Yih-Choung Yu. Control issues in rotary heart assist devices. In *Proceedings of the 2000*

American Control Conference. ACC (IEEE Cat. No. 00CH36334), volume 5, pages 3473–3477. IEEE, 2000.

[6] B Deswysen, A A Charlier, and Michel Gevers. Quantitative evaluation of the systemic arterial bed by parameter estimation of a simple model. *Medical and Biological Engineering and Computing*, 18(2):153–166, 1980.

[7] Rached Dhaouadi, Ned Mohan, and Lars Norum. Design and implementation of an extended Kalman filter for the state estimation of a permanent magnet synchronous motor. *IEEE Transactions on Power Electronics*, 6(3):491–497, 1991.

[8] Arthur Gelb. *Applied optimal estimation*. MIT press, 1974.

[9] Jeffrey R Gohean. *Heirarchical Control of a Two-Piston Toroidal Pump*. PhD thesis, University of Texas at Austin, 2019.

[10] Jeffrey R. Gohean, Mitchell J. George, Kay Won Chang, Erik R. Larson, Thomas D. Pate, Mark Kurusz, Raul G. Longoria, and Richard W. Smalling. Preservation of native aortic valve flow and full hemodynamic support with the TORVAD using a computational model of the cardiovascular system. *ASAIO Journal*, 61(3):259–265, 2015.

[11] Jeffrey R Gohean, Mitchell J George, Thomas D Pate, Mark Kurusz, Raul G Longoria, and Richard W Smalling. Verification of a computational cardiovascular system model comparing the hemodynamics of a continuous flow to a synchronous valveless pulsatile flow left ventricular

assist device. *ASAIO journal (American Society for Artificial Internal Organs: 1992)*, 59(2):107, 2013.

[12] Daniel J. Goldstein, Mehmet C. Oz, and Eric A. Rose. Implantable Left Ventricular Assist Devices. *New England Journal of Medicine*, 339(21):1522–1533, 1998.

[13] M Grewal and K Glover. Identifiability of linear and nonlinear dynamical systems. *IEEE Transactions on automatic control*, 21(6):833–837, 1976.

[14] Clinton D. Kemp and John V. Conte. The pathophysiology of heart failure. *Cardiovascular Pathology*, 21(5):365–371, 2012.

[15] George V. Letsou, Thomas D. Pate, Jeffrey R. Gohean, Mark Kurusz, Raul G. Longoria, Larry Kaiser, and Richard W. Smalling. Improved left ventricular unloading and circulatory support with synchronized pulsatile left ventricular assistance compared with continuous-flow left ventricular assistance in an acute porcine left ventricular failure model. *Journal of Thoracic and Cardiovascular Surgery*, 140(5):1181–1188, 2010.

[16] Lennart Ljung. Asymptotic behavior of the extended Kalman filter as a parameter estimator for linear systems. *IEEE Transactions on Automatic Control*, 24(1):36–50, 1979.

[17] Jairo Melo and Jay I. Peters. Low systemic vascular resistance: Differential diagnosis and outcome. *Critical Care*, 3(3):71–77, 1999.

[18] P Molino, C Cerutti, C Julien, G Cuisinaud, M P Gustin, and C Paultre. Beat-to-beat estimation of windkessel model parameters in conscious rats. *The American journal of physiology*, 274(1 Pt 2):H171–7, 1998.

[19] M. M. Parker, J. H. Shelhamer, C. Natanson, D. W. Alling, and J. E. Parrillo. Serial cardiovascular variables in survivors and nonsurvivors of human septic shock: Heart rate as an early predictor of prognosis, 1987.

[20] Anatol Prinzing, Ulf Herold, Anna Berkefeld, Markus Krane, Rüdiger Lange, and Bernhard Voss. Left ventricular assist devices-current state and perspectives. *Journal of Thoracic Disease*, 8(8):E660–E666, 2016.

[21] Gerson Rosenberg, W. M. Phillips, D. L. Landis, and W. S. Pierce. Design and evaluation of the pennsylvania state university mock circulatory system. *ASAIO Journal*, 4(2):41–49, 1 1981.

[22] Timothy L. Ruchti, Ronald H. Brown, Dean C. Jeutter, and Xin Feng. Identification algorithm for systemic arterial parameters with application to total artificial heart control. *Annals of Biomedical Engineering*, 21(3):221–236, 2006.

[23] David G. Silverman, Ala S. Haddadin, Robert G. Stout, Kirk H. Shelley, Aymen A. Awad, Tarek M. Badr, and Hossam Tantawy. The relationship between the photoplethysmographic waveform and systemic vascular resistance. *Journal of Clinical Monitoring and Computing*, 21(6):365–372, 2007.

[24] Marwin A. Simaan, Antonio Ferreira, Shaohui Chen, James F. Antaki, and David G. Galati. A dynamical state space representation and performance analysis of a feedback-controlled rotary left ventricular assist device. *IEEE Transactions on Control Systems Technology*, 17(1):15–28, 2009.

[25] By Miltiadis A Stefadouros, Michael J Dougherty, and William Grossman. Determination of systemic vascular resistance. *Circulation*, 47:101–107, 1973.

[26] N Stergiopulos, P Segers, and N Westerhof. Use of pulse pressure method for estimating total arterial compliance in vivo. *American Journal of Physiology*, 276(2 Pt 2):H424–8, 1999.

[27] E A Wan and R Van Der Merwe. The unscented Kalman filter for nonlinear estimation. In *Proceedings of the IEEE 2000 Adaptive Systems for Signal Processing, Communications, and Control Symposium (Cat. No.00EX373)*, pages 153–158, 2000.

[28] Nico Westerhof, Jan Willem Lankhaar, and Berend E. Westerhof. The arterial windkessel. *Medical and Biological Engineering and Computing*, 47(2):131–141, 2009.

[29] World Health Organization. Noncommunicable diseases country profiles 2018. Technical report, World Health Organization, 2018.

[30] Yi Wu, Paul E Allaire, Gang Tao, and Don Olsen. Modeling, estimation, and control of human circulatory system with a left ventricular assist device. *IEEE Transactions on Control Systems Technology*, 15(4):754–767, 2007.

[31] Yih Choung Yu, Robert Boston, Marwan A. Simaan, and James F. Antaki. Minimally invasive estimation of systemic vascular parameters. *Annals of Biomedical Engineering*, 29(7):595–606, 2001.